Directed Sub-Terahertz Neural Disruption System: RF Chain Design, Pulse Architectures, and Man-Portable Implementation at 100–300 GHz

Jacob Wohl
CTO at Calvexa Group, LLC
Email: Jacob@IRISC2.com

***Abstract*—This paper presents the engineering design of a directed sub-terahertz (sub-THz) neural disruption system optimized for producing vestibular disorientation, nausea, cognitive degradation, and autonomic disturbance in targeted subjects at standoff range. The system generates pulse-modulated electromagnetic radiation at 100–300 GHz carrier frequencies, with pulse repetition frequencies (PRFs) precisely matched to the spectral bands of human neural oscillations most associated with disorienting physiological effects: alpha (8–13 Hz) for vestibular disruption and nausea induction, beta sub-bands (12.5–30 Hz) for cognitive interference and motor impairment, and cross-frequency architectures for compounding multi-system disorientation. Three pulse modulation architectures are implemented—continuous pulse trains for sustained neural rhythm disruption, neural-waveform envelope modulation for maximal entrainment efficacy, and burst-mode pulsing that replicates pathological thalamocortical discharge patterns associated with absence seizure and vestibular crisis phenomenology. The neurophysiological basis for each disruption modality is developed in detail, including the thalamocortical pacemaker vulnerability to external entrainment, vestibular nucleus sensitivity to alpha-rate afferent perturbation, beta sub-band selectivity for motor versus cognitive degradation, and multi-modal synergistic enhancement via simultaneous pulsed ultrasonic stimulation. The RF chain employs a BNC Model 871 51 GHz source, Schottky diode frequency multiplier chains, EIK power amplification, and Cassegrain reflector antennas achieving EIRP exceeding $100\,\mathrm{dBm}$ in sub-degree pencil beams. Detailed disruption-optimized pulse protocols, effect-specific frequency targeting strategies, and dose–response analyses are provided.**

***Index Terms*—Sub-terahertz, neural disruption, directed energy, vestibular disorientation, nausea induction, cognitive degradation, neural entrainment, pulse modulation, alpha rhythm disruption, beta sub-band targeting, thalamocortical perturbation, multi-modal stimulation, burst-mode pulsing, neuroelectromagnetics, directed neural effects**

I. Introduction

THE human brain operates through a hierarchy of electrical oscillations spanning approximately 0.5 Hz to 100 Hz, organized into canonical frequency bands—delta, theta, alpha, beta, and gamma—each governing distinct cognitive states, sensorimotor coordination, vestibular processing, and autonomic regulation [1], [2]. Critically, the *disruption* of these oscillations—through external entrainment, desynchronization, or pathological forcing—produces specific, predictable neurological deficits: alpha-band perturbation drives nausea and vestibular disorientation; beta-band interference degrades motor coordination and cognitive function; and cross-frequency decoupling fragments the integrative processes that maintain spatial awareness and equilibrium [7], [13], [14]. These oscillatory vulnerabilities represent an exploitable pathway for directed, non-contact neurological disruption.

The principle that externally applied energy, temporally structured to match neural oscillation frequencies, can produce disorienting physiological effects has been demonstrated across multiple energy modalities. Bovill established that visible light strobed at 10–30 Hz (the alpha–beta range) produces the *bucha* or *flicker* effect—nausea, vertigo, giddiness, and cognitive incapacitation—in a significant fraction of the exposed population [17], [18]. Frey demonstrated that pulsed microwave radiation at $\sim$1.3 GHz induces perceived auditory sensations through thermoelastic cranial expansion [10], [16]. Most directly relevant to the present work, Norris and Putterman demonstrated that electromagnetic waveforms in the 300 MHz–300 GHz range, pulsed at alpha (8–12 Hz) and beta (12.5–30 Hz) frequencies, produce nausea, cognitive disturbance, vertigo, and general disorientation in targeted subjects [12]. Their work further established a critical finding: synergistic enhancement of these discombobulating effects occurs when pulsed electromagnetic and pulsed ultrasonic ($>$20 kHz) waveforms are simultaneously delivered, with a 10–50 ms inter-modality phase offset compensating for differential neural processing latencies.

These findings—spanning visual, microwave, and ultrasonic modalities—converge on a single principle: **the temporal modulation pattern of an energy stimulus, not its carrier frequency or average intensity, is the primary determinant of neurological disruption efficacy.** The carrier frequency determines the delivery mechanism (tissue penetration, absorp-

tion profile, range); the PRF determines *which* neural systems are disrupted and *how*.

This paper presents the complete engineering design of a directed sub-THz system optimized to exploit this principle, delivering precision neural-rate-pulsed EM radiation to produce targeted discombobulating effects at standoff range. The system:

(i) Generates a phase-coherent sub-THz carrier in the 100–300 GHz range via frequency multiplication from a 51 GHz baseband source (BNC Model 871);
(ii) Amplifies the carrier to watt-level peak power using solid-state and vacuum electronic amplifiers;
(iii) Applies precision pulse modulation at PRFs spanning the disruption-relevant neural bands (alpha through beta: 8–30 Hz), with extensions to delta (0.5–4 Hz) for autonomic disruption and gamma (30–100 Hz) for perceptual fragmentation;
(iv) Implements three pulse architectures optimized for different disruption modalities: sustained rhythm forcing, neural-waveform entrainment, and pathological burst-mode pulsing;
(v) Radiates the modulated signal through high-gain directional antennas with EIRP exceeding $80\,\mathrm{dBm}$, producing sub-degree pencil beams for individual targeting at range.

This document details the complete engineering design of a system that:

(i) Generates a phase-coherent sub-THz carrier in the 100–300 GHz range via frequency multiplication from a 51 GHz baseband source (BNC Model 871);
(ii) Amplifies the carrier to watt-level power using solid-state and vacuum electronic amplifiers;
(iii) Applies precision pulse modulation at PRFs spanning the full range of human neural oscillation frequencies (0.5–100 Hz), with extensions to higher cortical ripple frequencies (100–600 Hz);
(iv) Implements three distinct pulse architectures: continuous pulse trains, neural-waveform envelope modulation, and burst-mode pulsing with configurable timing parameters;
(v) Radiates the modulated signal through high-gain directional antenna systems with EIRP exceeding $80\,\mathrm{dBm}$.

A. Neural Oscillation Frequency Bands

Table I summarizes the canonical neural oscillation bands, their frequency ranges, associated cognitive/physiological correlates, and the corresponding pulse periods for the EM system.

B. Fundamental System Concept

The system concept is illustrated schematically in Fig. 1. A high-frequency electromagnetic carrier (100–300 GHz) is pulse-modulated such that discrete packets of EM energy are delivered at repetition rates matching specific neural oscillation frequencies. The carrier frequency determines the wavelength, tissue interaction depth, and absorption coefficient; the pulse repetition frequency determines the temporal pattern of energy delivery at neural timescales.

TABLE I: Neural Oscillation Bands, Correlates, and Disruption Effects When Externally Entrained

Band	Range	Correlate	Disruption Effect
δ	0.5–4 Hz	Deep sleep, autonomic	Autonomic dysregulation, drowsiness
θ	4–8 Hz	Navigation, memory	Spatial disorientation, memory disruption
α	8–13 Hz	Thalamic idle, vestib.	**Nausea, vertigo, vestibular crisis**
β	13–30 Hz	Motor, cognition	Motor impairment, cognitive degradation
γ	30–100 Hz	Binding, attention	Perceptual fragmentation, confusion

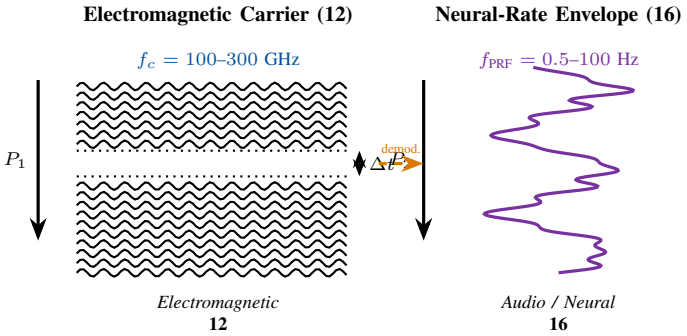

Fig. 1: Fundamental system concept after the reference diagrams. **Left (12)**: Sub-THz electromagnetic carrier consisting of pulse bursts propagating in direction P_1, with inter-pulse gap Δt determining the neural-rate PRF. **Right (16)**: The resulting neural-rate temporal envelope (direction P_2), exhibiting the complex waveform morphology characteristic of neural oscillations. The envelope frequency f_{PRF} is matched to target neural oscillation bands (δ, θ, α, β, γ).

C. Document Organization

The remainder of this document is organized as follows. Section II provides a detailed analysis of the neural oscillation pulse timing requirements and the three pulse architectures. Section III presents the neurophysiological basis for neural-rate targeting, including entrainment theory, multi-modal interaction mechanisms, and known physiological responses. Section IV describes the baseband signal source. Section V covers frequency upconversion. Section VI addresses power amplification. Section VII details the pulse modulation implementation hardware. Section VIII presents directional antenna systems. Section IX integrates these into complete system configurations. Section X presents a man-portable system design with SWaP analysis and field-deployable form factors. Section XI discusses bioelectromagnetic considerations. Section XIII covers safety protocols. Section XIV provides cost estimates.

II. Neural Oscillation Pulse Architecture

The core innovation of this system is the precise mapping of neural oscillation temporal dynamics—particularly those governing vestibular processing, motor coordination, and cognitive integration—onto the pulse modulation structure of a sub-THz electromagnetic carrier. Three distinct pulse architectures are

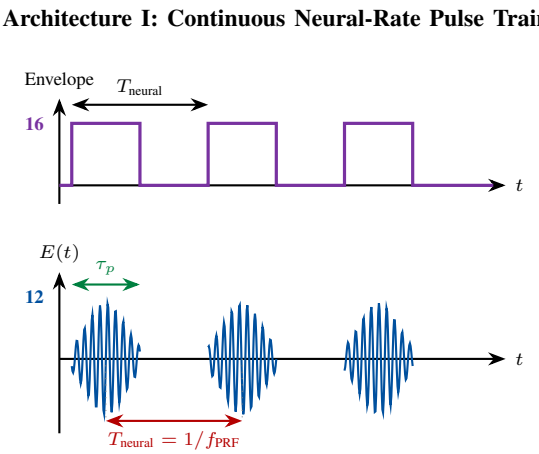

Fig. 2: Architecture I: Continuous pulse train. The sub-THz carrier (**12**, blue) is gated into discrete pulses of width τ_p at a PRF equal to the target neural oscillation frequency. The envelope (**16**, purple) is a periodic rectangular function with period $T_{\text{neural}} = 1/f_{\text{PRF}}$.

TABLE II: Architecture I Parameters for Each Neural Band ($\delta = 10\%$, $f_c = 150$ GHz)

Band	f_{PRF}	T_{neural}	τ_p	N_c	Δt
δ	2 Hz	500 ms	50 ms	7.5×10^9	450 ms
θ	6 Hz	167 ms	16.7 ms	2.5×10^9	150 ms
α	10 Hz	100 ms	10 ms	1.5×10^9	90 ms
β	20 Hz	50 ms	5 ms	7.5×10^8	45 ms
γ	60 Hz	16.7 ms	1.67 ms	2.5×10^8	15 ms
γ_h	100 Hz	10 ms	1 ms	1.5×10^8	9 ms

defined, each optimized for different disruption modalities and escalation profiles.

A. Architecture I: Continuous Pulse Train at Neural PRF

The simplest architecture applies a continuous periodic pulse train to the sub-THz carrier at a PRF equal to the target neural oscillation frequency. Each pulse consists of a burst of N_c carrier cycles at frequency f_c.

The pulse parameters for Architecture I (Fig. 2) are fully specified by:

$$f_{\text{PRF}} = f_{\text{neural}} \text{ (target band center)} \quad (1)$$

$$T_{\text{neural}} = 1/f_{\text{PRF}} \quad (2)$$

$$\tau_p = \delta \cdot T_{\text{neural}} \text{ (pulse width)} \quad (3)$$

$$N_c = \tau_p \cdot f_c \text{ (cycles per pulse)} \quad (4)$$

where δ is the duty cycle. Table II provides specific values for each neural band.

The inter-pulse gap $\Delta t = T_{\text{neural}} - \tau_p$ is the critical timing parameter shown in the reference diagrams. It defines the period of zero EM field exposure between successive pulse deliveries. For alpha-band targeting at 10 Hz, $\Delta t = 90$ ms; each pulse delivers 1.5×10^9 carrier cycles in a 10 ms window.

B. Architecture II: Neural Waveform Envelope Modulation

Architecture II goes beyond simple rectangular pulsing to reproduce the actual amplitude envelope morphology of neural oscillations. Rather than gating the carrier on/off, the carrier amplitude is continuously modulated by a waveform that replicates the temporal structure of a target neural rhythm.

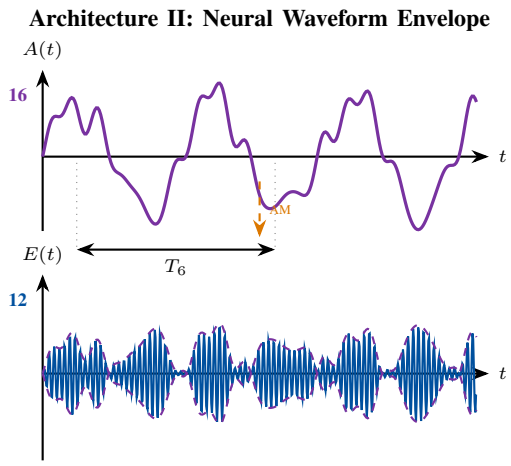

Fig. 3: Architecture II: Neural waveform envelope modulation. **Top (16)**: Recorded or synthesized neural oscillation waveform serving as the AM envelope, with period T_6. **Bottom (12)**: Sub-THz carrier amplitude-modulated by the neural waveform. The dashed purple curves show the instantaneous envelope. This architecture preserves the complex morphology of neural rhythms including cross-frequency coupling.

Architecture II (Fig. 3) is mathematically described by:

$$E(t) = A_{\text{neural}}(t) \cdot \cos(2\pi f_c t + \phi_c) \quad (5)$$

where $A_{\text{neural}}(t)$ is the neural oscillation waveform, which may be:

- A single sinusoid: $A(t) = A_0[1 + m\sin(2\pi f_{\text{neural}} t)]$
- A sum of harmonically related oscillations modeling cross-frequency coupling:

$$A(t) = A_0 \left[1 + \sum_k m_k \sin(2\pi f_k t + \phi_k)\right] \quad (6)$$

- A digitized recording of actual EEG/LFP data replayed from an arbitrary waveform generator.

The period T_6 corresponds to the fundamental period of the neural waveform envelope. This architecture is particularly suited for investigating cross-frequency coupling phenomena (e.g., theta-gamma coupling [5]), where the gamma-band amplitude is modulated by the theta-band phase.

C. Architecture III: Burst-Mode Pulsing

Architecture III, shown in Fig. 4, is the most potent disruption-optimized pulse structure. It mirrors the *burst firing* patterns observed in thalamocortical relay neurons during pathological states—absence seizures, vestibular crisis, and sleep–wake transition instability [6]. By replicating these pathological discharge patterns in the EM domain, Architecture III is designed to force the thalamocortical system into oscillatory modes associated with maximal disorientation. The

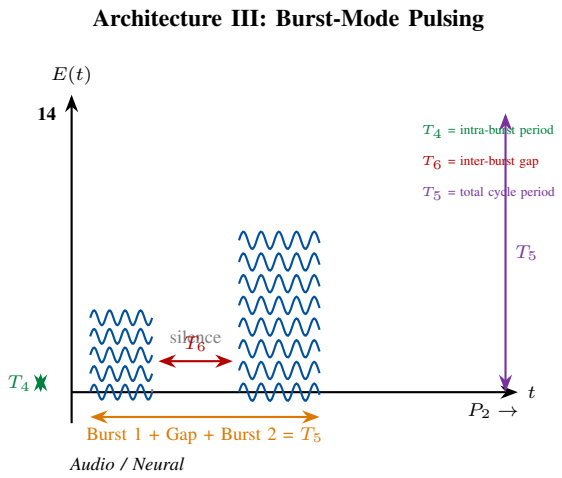

Fig. 4: Architecture III: Burst-mode pulsing after the reference diagrams. Element **14** shows the burst structure with three critical timing parameters: T_4 (intra-burst pulse period—the spacing between individual carrier pulses within a burst), T_6 (inter-burst silence period—the gap between successive bursts), and T_5 (total cycle period encompassing one complete burst-gap-burst sequence). This structure mirrors thalamocortical burst firing patterns.

waveform consists of discrete *pulse bursts*, each containing multiple carrier pulses at a fast intra-burst rate, separated by longer inter-burst intervals.

Architecture III is characterized by three independent timing parameters (referencing Fig. 4):

- T_4: **Intra-burst pulse period**. The time between successive carrier pulses *within* a single burst. This determines the fast oscillation frequency within the burst: $f_{\text{intra}} = 1/T_4$.
- T_5: **Total burst cycle period**. The time for one complete cycle of burst + inter-burst gap. The burst repetition frequency is $f_{\text{burst}} = 1/T_5$.
- T_6: **Inter-burst silence period**. The duration of zero EM emission between successive bursts. $T_6 = T_5 - T_{\text{burst,on}}$, where $T_{\text{burst,on}}$ is the burst active duration.

The burst-mode duty cycle is:

$$\delta_{\text{burst}} = \frac{T_{\text{burst,on}}}{T_5} = \frac{T_5 - T_6}{T_5} = 1 - \frac{T_6}{T_5} \tag{7}$$

1) Neuroscience-Motivated Burst Parameters: Table III maps specific neural phenomena to burst-mode timing configurations.

The thalamocortical burst configuration is particularly significant. During non-REM sleep, thalamic relay neurons fire in burst mode with 3–8 spikes at 200–400 Hz inter-spike frequency, recurring at 1–4 Hz (delta) or 7–14 Hz (spindle) rates [7]. Architecture III directly replicates this temporal structure in the EM domain.

D. Composite Multi-Band Architecture

For advanced experiments, Architectures I–III can be combined to create composite waveforms targeting multiple neural

TABLE III: Burst-Mode Configurations Mapped to Neural Phenomena

Neural Target	f_{burst}	T_5	f_{intra}	T_4	T_6
Thalamic burst	6 Hz	167 ms	300 Hz	3.3 ms	134 ms
Sleep spindle	12 Hz	83 ms	1 kHz	1 ms	63 ms
θ-γ coupl.	6 Hz	167 ms	60 Hz	16.7 ms	100 ms
α burst	10 Hz	100 ms	500 Hz	2 ms	80 ms
β burst	20 Hz	50 ms	2 kHz	0.5 ms	40 ms
Ripple burst	4 Hz	250 ms	200 Hz	5 ms	200 ms

TABLE IV: Required Pulse Timing Precision

Parameter	**Required**	**Achieved**
PRF accuracy	$< 0.1\%$	$< 0.001\%$ (AWG)
Pulse-to-pulse jitter	< 1 μs	< 100 ns (AWG)
Rise/fall time	$< T_4/10$	< 10 μs (BNC)
		< 10 ns (PIN)
		< 100 ns (EIK grid)
Amplitude stability	$< 1\%$	$< 0.5\%$ (PA)

bands simultaneously:

$$A(t) = \sum_i w_i \cdot B_i(t; T_{4,i}, T_{5,i}, T_{6,i}) \tag{8}$$

where B_i are individual burst waveforms at different neural frequencies and w_i are weighting coefficients. This enables investigation of cross-frequency entrainment hypotheses.

E. Timing Precision Requirements

Neural oscillations exhibit temporal jitter of ± 5–20% around their nominal period. The EM pulse system must achieve significantly better timing precision to serve as a controlled stimulus:

All three modulation hardware approaches (Section VII) exceed these requirements by substantial margins.

III. Neurophysiological Basis and Interaction Mechanisms

The pulse architectures defined in Section II are grounded in the electrophysiology of neural oscillation generation, the biophysics of EM–tissue interaction, and the emerging understanding of neural entrainment by external energy sources. This section provides the scientific basis for the system's neural-rate targeting strategy.

A. Neural Oscillation Electrophysiology

1) Thalamocortical Pacemaker Mechanisms: The alpha rhythm (8–12 Hz), which serves as one of the primary targeting bands for the present system, is generated predominantly by the rhythmic burst firing of thalamocortical relay neurons in the thalamus [13], [7]. These neurons possess intrinsic membrane properties—specifically, a low-threshold calcium conductance (I_T) and a hyperpolarization-activated cation current (I_h)—that produce self-sustaining oscillations in the 8–12 Hz range. The thalamic reticular nucleus provides

GABAergic inhibition that synchronizes populations of relay cells, giving rise to the large-amplitude, spatially coherent alpha oscillations observable on the scalp via EEG.

This pacemaker architecture has a critical implication for external entrainment: because the oscillation frequency is determined by intrinsic membrane time constants (the interplay of I_T and I_h), perturbations that modulate membrane potential, intracellular calcium dynamics, or synaptic input timing at the appropriate phase can shift the oscillation frequency toward the external driving frequency—a process known as *neural entrainment* [21], [22].

2) Beta Sub-Band Structure: Beta oscillations (12.5–30 Hz) exhibit a finer functional sub-band structure than other neural rhythms [14], [15]:

- **Low beta (12.5–16 Hz)**: Associated with relaxed sensorimotor idling and the post-movement beta rebound. These oscillations are strongest over motor cortex and can be modulated by somatosensory input.
- **Mid-beta (16.5–20 Hz)**: Linked to sustained attention, working memory maintenance, and sensory gating. Mid-beta power increases during cognitive load.
- **High beta (20.5–28 Hz)**: Associated with active motor planning, anxiety-related cortical activation, and pathological states. Excessive high beta is a marker of anxiety disorders.

This sub-band structure implies that a neural-rate pulsed EM system must achieve fine frequency resolution within the beta band ($<$1 Hz steps) to selectively target distinct functional states. The BNC 871's frequency resolution of $<$0.001 Hz (Section IV) far exceeds this requirement.

3) Gamma Oscillations and Binding: Gamma oscillations (30–100 Hz) are generated by the interplay of excitatory pyramidal neurons and fast-spiking inhibitory interneurons (particularly parvalbumin-positive basket cells) through a mechanism known as the pyramidal-interneuron gamma (PING) circuit [19], [20]. Gamma rhythms are critical for:

- Perceptual binding (integrating features into coherent percepts)
- Selective attention and sensory gain control
- Cross-regional cortical communication
- Working memory encoding

The fast inhibitory time constants governing gamma generation ($\sim$10–30 ms GABAergic decay) make these oscillations particularly sensitive to perturbation by precisely timed external stimuli. Disruption of gamma synchrony fragments perceptual binding, producing subjective confusion and an inability to form coherent percepts—a key component of the discombobulation response.

B. Vestibular System Vulnerability to Alpha-Rate Perturbation

The vestibular system is the primary target for inducing nausea, vertigo, and spatial disorientation. The vestibular nuclei in the brainstem exhibit strong oscillatory activity in the alpha band (8–12 Hz), reflecting their coupling to the thalamocortical alpha rhythm via the vestibulothalamic projection through the ventral posterolateral (VPL) and ventral posteromedial (VPM) thalamic nuclei [30]. This anatomical coupling creates a specific vulnerability: external forcing of the alpha rhythm—whether by visual flicker (bucha effect), pulsed EM, or pulsed ultrasound—propagates through thalamocortical circuits to the vestibular processing network.

The resulting *sensory conflict* between externally entrained vestibular signals and veridical proprioceptive/visual input is the primary mechanism for nausea and vertigo induction. This is functionally identical to motion sickness, where conflicting sensory signals regarding head position and movement trigger the emetic response via the nucleus tractus solitarius and area postrema [31], [32]. The critical parameters for maximizing vestibular disruption are:

- **PRF**: 8–12 Hz (alpha band), with 10 Hz as the empirically most effective frequency [12], [17]
- **Sweep**: $\pm$2 Hz around 10 Hz at 0.2–1 Hz sweep rate to capture individual alpha frequency variability
- **Duty cycle**: 10–50%, with higher duty cycles producing more rapid onset
- **Duration to effect**: 10–60 s for initial nausea onset; 1–5 min for sustained vertigo

C. Cognitive and Motor Disruption via Beta-Band Targeting

Beta-band disruption (12.5–30 Hz) targets the sensorimotor and prefrontal cortical networks responsible for motor planning, sustained attention, and executive function. Each beta sub-band produces distinct degradation profiles:

- **Low beta (12.5–16 Hz)**: Disruption of the post-movement beta rebound impairs motor sequencing and fine motor control. The subject experiences clumsiness, difficulty with coordinated movements, and impaired gait.
- **Mid-beta (16.5–20 Hz)**: Interference with sustained attention and working memory maintenance. The subject experiences difficulty concentrating, confusion, and inability to follow multi-step tasks.
- **High beta (20.5–28 Hz)**: Forced entrainment of high beta oscillations mimics the cortical signature of acute anxiety, producing subjective distress, hypervigilance, and panic-like autonomic activation (tachycardia, diaphoresis) without an identifiable external cause [14].

Simultaneous alpha and beta disruption—achievable via Architecture II (neural waveform envelope) or composite multi-band Architecture—produces compound discombobulation: vestibular nausea combined with cognitive confusion and motor impairment, rendering the subject unable to effectively respond or identify the source of the disturbance.

D. Neural Entrainment Theory

1) Resonance and Arnold Tongues: Neural oscillators, like all nonlinear oscillators, exhibit frequency-locking (entrainment) when driven by an external periodic stimulus whose frequency falls within a capture range (Arnold tongue) of the natural oscillation frequency [23]. The width of the Arnold tongue—i.e., the range of driving frequencies over which entrainment occurs—increases with stimulus amplitude:

$$\Delta f_{\text{capture}} \propto A_{\text{stim}}^{1/2} \tag{9}$$

where A_{stim} is the effective stimulus amplitude perceived by the neural oscillator.

For electromagnetic neural-rate pulsing, the effective stimulus amplitude depends on the coupling pathway (thermal, mechanotransductive, or direct field effect) and the power density at the tissue surface. The present system's high EIRP and narrow beamwidth maximize the on-axis power density, thereby maximizing the capture range for potential entrainment.

2) Phase-Dependent Susceptibility: Neural oscillations exhibit phase-dependent excitability: the response to an external perturbation depends critically on the instantaneous phase of the endogenous oscillation at which the perturbation arrives [24], [25]. During the depolarizing (excitable) phase, even weak perturbations can advance or delay the oscillation cycle, while during the hyperpolarized (refractory) phase, much stronger stimuli are required. This phase-response curve (PRC) characteristic implies that:

1) Continuous periodic stimulation (Architecture I) will gradually align its pulses with the susceptible phase, achieving steady-state entrainment.
2) Burst-mode stimulation (Architecture III) may be more effective than continuous pulsing because the inter-burst silence allows the oscillator to relax toward its natural dynamics, increasing the phase window for subsequent burst arrival.

3) Frequency Sweep Strategy for Resonance Identification: Because the precise endogenous oscillation frequency varies both across individuals and temporally within a single individual (alpha frequency, for example, ranges from ∼8 Hz to ∼12 Hz depending on alertness and genetic factors [26]), a fixed-frequency pulse train may not achieve optimal entrainment. The patent literature describes a sweep strategy in which the PRF is continuously varied within the target band, cycling through the full range every 1–5 seconds [12]. This ensures that the driving frequency periodically coincides with the subject's instantaneous natural frequency, facilitating repeated capture events.

An alternative approach is discrete frequency stepping, where the PRF is set to individual candidate frequencies and held until a response is observed (or a timeout elapses), then advanced to the next candidate. This method sacrifices speed for precision in resonance identification.

Both strategies are supported by the present system's LabVIEW-controlled AWG architecture (Section VII), which enables arbitrary frequency profiles with sub-Hz resolution.

E. Multi-Modal Interaction: Electromagnetic and Acoustic Pathways

1) Complementary Neural Coupling Pathways: Electromagnetic and acoustic energy couple to the nervous system through fundamentally different transduction mechanisms:

- **Electromagnetic (100–300 GHz)**: Absorbed in the superficial tissue layers (0.1–0.4 mm), generating thermal transients detected by thermoreceptive C-fibers and Aδ-fibers in the skin. Afferent signals propagate via the spinothalamic tract to the thalamus and somatosensory cortex.
- **Ultrasonic (>20 kHz)**: Induces mechanical pressure oscillations in tissue, activating mechanosensitive ion channels (e.g., Piezo1, TRPA1) and potentially stimulating vestibular receptors. Coupling occurs through both direct cochlear stimulation (via bone conduction at sufficiently high intensities) and somatosensory mechanoreception.

When both modalities are pulsed at the same neural-rate frequency, they converge on thalamocortical circuits through independent afferent pathways (somatosensory and auditory/vestibular), potentially producing a synergistic effect on neural entrainment that exceeds either modality alone [12], [27].

2) Phase Offset Between Modalities: Because electromagnetic and acoustic stimuli are processed by neural circuits with different latencies (electromagnetic thermal transduction: ∼50–200 ms; auditory processing: ∼10–50 ms), achieving temporal coincidence at the cortical level requires introducing a deliberate phase offset $\Delta\phi$ between the two pulse trains:

$$\Delta\phi = 2\pi f_{\text{PRF}} \cdot \Delta t_{\text{latency}} \tag{10}$$

where $\Delta t_{\text{latency}} \approx 10$–$50$ ms is the differential neural processing latency [12]. For alpha-band pulsing at $f_{\text{PRF}} = 10$ Hz ($T = 100$ ms), a 25 ms offset corresponds to a phase advance of $\pi/2$ radians for the acoustic waveform relative to the electromagnetic.

3) Power Density and Range Considerations: Prior work at lower carrier frequencies (1–10 GHz) established effective power density thresholds on the order of 0.3 mW/cm^2 average, with peak pulse power densities of 0.3 W/cm^2 [12]. At sub-THz frequencies (100–300 GHz), the shallower penetration depth concentrates the absorbed energy in a thinner tissue layer, potentially achieving equivalent volumetric energy deposition at lower incident power densities:

$$\text{SAR}_{\text{vol}} = \frac{S \cdot (1 - |R|^2)}{\rho \cdot \delta_p} \tag{11}$$

where S is the incident power density, $|R|^2$ is the surface reflection coefficient, ρ is the tissue density, and δ_p is the penetration depth. Since δ_p at 200 GHz (∼0.15 mm) is roughly 50× smaller than at 2 GHz (∼8 mm), an incident power density 50× lower can produce equivalent volumetric absorption.

F. Known Physiological Responses to Neural-Rate Pulsed EM Exposure

Table V summarizes the physiological effects reported in the literature and patent disclosures for EM energy pulsed at neural oscillation frequencies.

The most consistently reported effects are associated with alpha-band (8–12 Hz) pulsing, consistent with the alpha rhythm's generation by thalamic pacemaker circuits that are susceptible to external perturbation. Beta sub-band targeting (particularly 12.5–16 Hz) has shown effects on motor coordination, aligning with the known role of sensorimotor beta in movement planning and execution [14].

TABLE V: Reported Physiological Responses to Neural-Rate Pulsed EM Stimulation

PRF Band	Effect	Carrier	Reference
α (8–12 Hz)	Nausea, cognitive disruption, vertigo	1–10 GHz	[12]
α–β (10–30 Hz)	Flicker/bucha effect (visual)	Visible	[17]
Low β (12.5–16 Hz)	Motor disruption	1–10 GHz	[12]
Broadband pulsed	Auditory percept (Frey effect)	1.3 GHz	[10]
α (10 Hz), CW carrier	EEG entrainment	450 MHz	[3]
α (10 Hz)	Enhanced effect w/ ultrasonic	1–10 GHz + 40–50 kHz	[12]

TABLE VI: BNC Model 871-50 Signal Generator Specifications

Parameter	Value
Frequency range	1 kHz – 51 GHz
Resolution	$<$0.001 Hz
Power range	-120 to $+20$ dBm
Power resolution	0.01 dB
Switching speed	10 µs
Pulse modulation	Internal
On/off ratio	$>$80 dB
Min. pulse width	10 µs
AM modulation (MOD opt.)	External input
Bandwidth	$>$100 kHz
Remote control	Ethernet, USB, GPIB
LabVIEW drivers	Native
Reference	Internal OCXO
External ref.	1–250 MHz
Phase noise (est.)	-95 dBc/Hz @ 10 kHz

IV. Baseband Signal Source: BNC Model 871

The Berkeley Nucleonics Corporation (BNC) Model 871 signal generator series serves as the coherent baseband source.

A. Key Specifications

B. Frequency Multiplication to Target Bands

The 51 GHz output enables direct multiplication to all target sub-THz frequencies:

$$f_{\times 2} = 102 \text{ GHz (W-band)} \tag{12}$$

$$f_{\times 3} = 153 \text{ GHz (D-band)} \tag{13}$$

$$f_{\times 4} = 204 \text{ GHz (G-band)} \tag{14}$$

$$f_{\times 6} = 306 \text{ GHz (Y-band)} \tag{15}$$

Phase noise degrades with multiplication factor N:

$$\mathcal{L}_{\text{out}}(f_m) = \mathcal{L}_{\text{in}}(f_m) + 20\log_{10}(N) \text{ dB} \tag{16}$$

C. Neural PRF Compatibility

The BNC 871's modulation capabilities are well-matched to neural oscillation frequencies:

TABLE VII: Frequency Multiplication Configurations

Target Band	N	Chain	f_{out} (GHz)	P_{out} (typ.)	PN deg. (dB)
W	$\times 2$	D	102	+3 dBm	6.0
D	$\times 3$	T	153	-2 dBm	9.5
G	$\times 4$	D+D	204	-5 dBm	12.0
Y	$\times 6$	D+T	306	-12 dBm	15.6

Input: +15 dBm at 51 GHz. PN deg. = phase noise degradation.

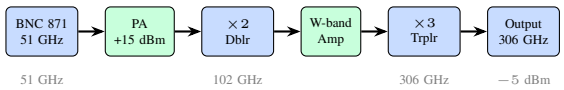

Fig. 5: VDI $\times 6$ amplifier-multiplier chain (AMC) with intermediate amplification at W-band.

- **Delta–gamma PRF (0.5–100 Hz)**: Periods of 10 ms to 2 s are vastly longer than the 10 µs switching time. Source-level pulse modulation is fully adequate.
- **Ripple PRF (100–600 Hz)**: Periods of 1.7–10 ms remain well within capability.
- **Intra-burst rate** (T_4-determined, up to several kHz): Supported by both internal pulse mode and external AM modulation.
- **External AM input**: Enables arbitrary neural waveform replay for Architecture II.

V. Frequency Upconversion

A. Schottky Diode Frequency Multipliers

GaAs Schottky barrier diode frequency multipliers generate harmonics of the input signal, with output waveguide filtering selecting the desired harmonic.

B. Amplifier-Multiplier Chains (AMCs)

Virginia Diodes Inc. (VDI) offers integrated AMCs with intermediate amplification stages:

C. Effect of Multiplication on Neural-Rate Modulation

A critical consideration: frequency multiplication preserves the pulse timing structure. If the 51 GHz carrier is pulsed at PRF $= 10$ Hz before multiplication, the output at 306 GHz is also pulsed at 10 Hz. However, AM modulation depth is affected:

- **On/off pulsing** (Architectures I, III): Multiplication has no effect on modulation integrity. The signal is either present or absent.
- **Analog AM** (Architecture II): The AM index m may be distorted by the nonlinear multiplier transfer function. Pre-distortion compensation or post-multiplier modulation is recommended.

D. Recommended Components

VI. Power Amplification

A. Technology Landscape

Fig. 6 maps the output power capabilities of the three principal amplifier technologies across the target frequency range.

TABLE VIII: Recommended Multiplier Components

Band	Config.	Vendor	Model
W	×2	VDI	WR10x2
		Eravant	SFA-W10
D	×3	VDI	WR6.5-AMC
G	×4	VDI	WR5.1-AMC
Y	×6	VDI	WR3.4-AMC

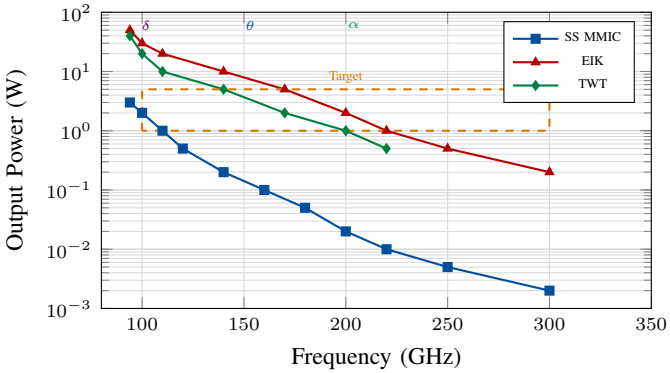

Fig. 6: Output power vs. frequency for solid-state MMIC (SS), extended interaction klystron (EIK), and traveling wave tube (TWT) amplifiers. Orange dashed box indicates the 1–5 W target region. Neural band labels at top indicate the carrier frequencies accessible via different multiplication factors from the 51 GHz source.

TABLE IX: W-band Solid-State PA Options

Vendor	P_{sat}	Gain	BW	Tech.
Eravant	0.5–1 W	20 dB	8 GHz	GaAs
Quinstar	1–2 W	25–35 dB	4 GHz	GaAs
NGMS	2–5 W	15 dB	10 GHz	GaN

TABLE X: CPI EIK Specifications at Target Frequencies

f (GHz)	P_{CW} (W)	P_{pk} (W)	Gain (dB)	V_b (kV)	Grid rise
94	20	1000–2000	35	15	50 ns
140	10–20	300–400	33	17	50 ns
170	5–10	50–100	30	18	80 ns
220	1.5–9	50–100	28	20	80 ns
264	0.7–5	10	25	22	100 ns
∼330†	0.1–0.2	0.5–1	22	24	100 ns

†Near upper limit of current CPI production (∼280 GHz). 330 GHz devices are developmental.

B. Solid-State MMIC Amplifiers (W-band)

For W-band (102 GHz), GaAs and emerging GaN MMIC power amplifiers provide 1–5 W output:

C. Extended Interaction Klystrons (EIKs)

CPI EIKs are the primary amplifier for D-band and above. Critical specifications for neural-rate pulsed operation:

The distinction between P_{CW} and P_{pk} is critical for neural-rate pulsed operation. CPI catalog peak power ratings (Table X) reflect rated pulsed duty cycles of 1–10%. At neural-rate PRFs (0.5–100 Hz), the extremely low duty cycles further relax thermal constraints:

$$P_{pk} = \frac{P_{avg,thermal}}{\delta_{burst}} \tag{17}$$

For example, at W-band (94 GHz), CPI pulsed EIKs deliver 1–2 kW peak power at 5–10% duty cycle. At 220 GHz, the VKY2462 provides **100 W peak** at 5% duty.

TABLE XI: Vacuum Electronic Device Support Infrastructure

Subsystem	Specification	Vendor
HV power supply	15–24 kV, regulated Arc-protected	CPI
Filament supply	Precision current, ramp-controlled	CPI
Water cooling	>1 L/min, 20±1°C	Lytron
Grid pulser	0–−500 V swing, <100 ns rise	CPI/Custom
Neural AWG	0.5–600 Hz output driving grid pulser	Keysight 33600A

D. EIK Grid-Pulsing for Neural-Rate Modulation

The EIK grid electrode provides the ideal mechanism for implementing all three neural pulse architectures directly at the high-power output stage:

- **Architecture I**: Periodic grid pulses at neural PRF (0.5–100 Hz). Trivially within grid pulser bandwidth.
- **Architecture II**: Analog grid bias modulation following the neural waveform envelope. Grid transfer characteristic maps bias voltage to beam current (and thus output power).
- **Architecture III**: Burst-mode grid pulsing. The grid pulser generates fast pulse trains (intra-burst rate up to several kHz) gated by slower burst-repetition-rate envelope. Grid rise time (<100 ns) supports intra-burst rates exceeding 1 MHz, vastly exceeding the fastest neural timing requirement ($T_4 \sim 0.5$ ms for 2 kHz intra-burst rate).

E. Infrastructure Requirements for VEDs

VII. Pulse Modulation Implementation

A. Modulation Hardware Architecture

Three hardware approaches implement the neural-rate pulse architectures, as shown in Fig. 7.

B. Approach A: Source-Level Modulation

The BNC 871 internal pulse mode gates the 51 GHz carrier at neural PRFs. An external arbitrary waveform generator (AWG) provides the pulse timing signal to the BNC 871 external trigger input.

Neural-rate performance:

- 10 ţs rise/fall time vs. minimum neural pulse period of 10 ms (gamma, 100 Hz): rise time is 0.1% of the period. **Excellent**.
- Pulse width of 10 ţs minimum supports intra-burst rates up to ∼50 kHz, far exceeding any neural frequency.
- On/off ratio >80 dB: clean neural pulsing with negligible inter-pulse leakage.

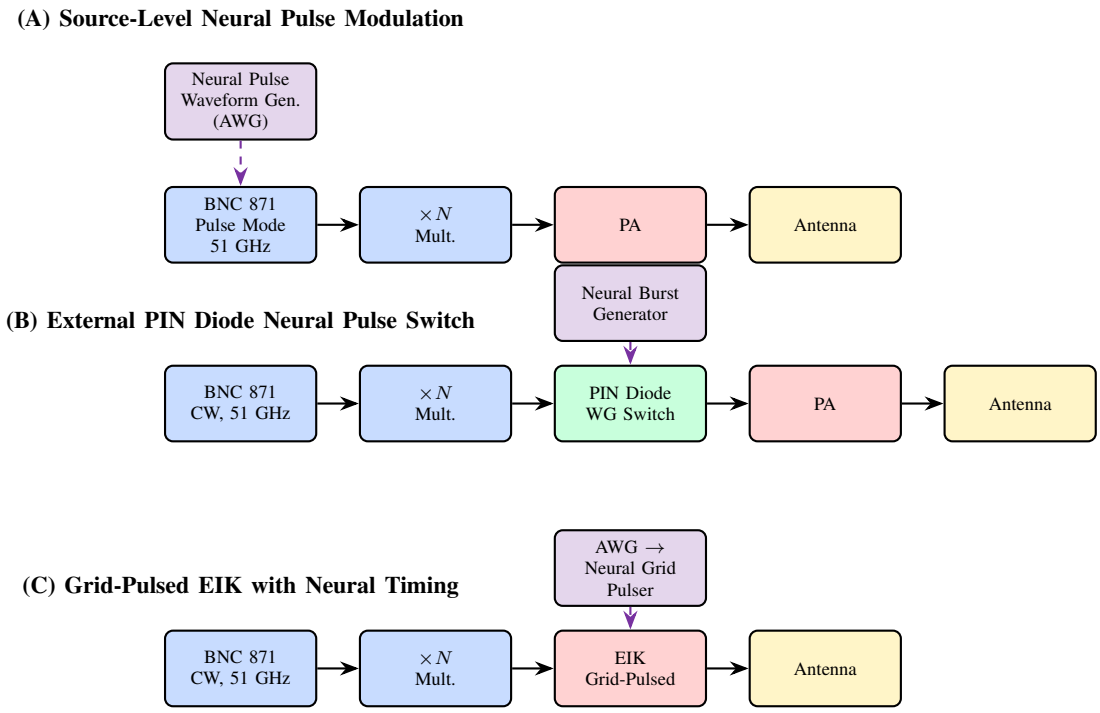

Fig. 7: Three pulse modulation hardware architectures for neural-rate operation. Purple dashed arrows indicate neural timing control signals. (A) Source-level modulation via BNC 871 pulse mode. (B) External PIN diode waveguide switch. (C) Grid-pulsed EIK—the *preferred approach* for Architectures I–III at maximum power.

TABLE XII: PIN Diode Modulator Specifications for Neural Pulsing

Parameter	Typical	Neural Req.
Rise/fall time	$<$10 ns	$<$1 ms
On/off ratio	20–40 dB	$>$20 dB
Insertion loss	1–3 dB	—
Max. PRF	$>$10 MHz	100 Hz (max)
Bandwidth	WR-10: 75–110	—
	WR-6.5: 110–170	—

C. Approach B: External PIN Diode Modulator

For Architectures I and III, a waveguide PIN diode switch provides the fastest, cleanest pulse modulation:

PIN diode switch response time ($<$10 ns) is approximately **six orders of magnitude** faster than required for gamma-band pulsing. This extraordinary margin ensures perfectly rectangular pulse edges with zero degradation of neural timing precision.

D. Approach C: Grid-Pulsed EIK (Preferred)

For maximum power delivery, the EIK grid is directly driven by the neural pulse waveform. A custom grid pulser circuit translates the low-voltage AWG output (typically 0–5 V) to the grid voltage swing (typically 0 to -300 V):

E. Neural Pulse Waveform Generation

The AWG generates the precise neural timing waveforms for all three architectures:

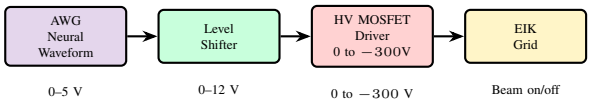

Fig. 8: Grid pulser signal chain for neural-rate EIK modulation. AWG generates the neural pulse waveform; HV MOSFET driver translates to grid voltage swing.

1) Architecture I Implementation:

```
Output: Square wave
Frequency: f_neural (0.5-100 Hz)
Duty cycle: delta (1-50%)
Amplitude: TTL (0-5V)
```

2) Architecture II Implementation:

```
Output: Arbitrary waveform
Source: Synthesized or recorded
        EEG/LFP waveform
Sample rate: >10 kHz
Bandwidth: DC to 600 Hz
Update: Real-time via USB/GPIB
```

3) Architecture III Implementation: The burst-mode waveform requires nested timing loops:

```
Outer loop: Period = T5 (burst rep.)
  Inner loop: Period = T4 (intra-burst)
    Pulse width: tau_p (carrier on)
  Duration: T5 - T6 (burst active)
Silence: T6 (inter-burst gap)
```

TABLE XIII: Antenna Gain and Beamwidth vs. Frequency/Aperture ($\eta_{\text{sys}} \approx 0.30$, including lens dielectric loss, surface errors, spillover, and feed mismatch)

f (GHz)	D (cm)	G (dBi)	HPBW	R_{ff} (m)
102	10	35	2.1°	6.8
102	30	45	0.7°	61
153	30	48	0.5°	92
153	50	53	0.3°	255
204	30	51	0.4°	122
306	20	50	0.3°	82
306	30	54	0.2°	184

Recommended AWG: Keysight 33600A Series (1 µHz to 120 MHz, 14-bit, 1 GSa/s, arbitrary waveform, LabVIEW compatible).

F. LabVIEW Integration for Neural Protocol Control

A unified LabVIEW control interface manages:

- BNC 871 carrier frequency and power
- AWG neural pulse waveform selection
- Real-time parameter adjustment (f_{PRF}, δ, T_4, T_5, T_6)
- Automated neural band sweep protocols
- Data logging and experiment sequencing
- Safety interlocks and emergency shutdown

VIII. Directional Antenna Systems

A. Antenna Gain Fundamentals

At sub-THz frequencies, high gain is achievable from physically small apertures:

$$G = \eta_{\text{sys}} \left(\frac{\pi D}{\lambda} \right)^2, \quad \theta_{3\text{dB}} \approx 70 \frac{\lambda}{D} \text{ (deg)} \tag{18}$$

where $\eta_{\text{sys}} \approx 0.30$ accounts for the aggregate of illumination taper, spillover, dielectric lens absorption, surface roughness loss, and feed mismatch at sub-THz frequencies—substantially below the nominal aperture efficiency $\eta_a \approx 0.55$ achievable at microwave bands.

B. Antenna Configurations

1) Corrugated Horn + Dielectric Lens: A corrugated conical horn feeds a plano-convex HDPE or TPX dielectric lens for gains of 40–50 dBi in a compact assembly. This is the recommended configuration for Configurations 1 and 3.

2) Cassegrain Reflector: A corrugated horn illuminates a precision Cassegrain dual-reflector system for maximum gain (50–65 dBi). Recommended for Configuration 2.

C. EIRP and Power Density

The EIRP for each configuration:

$$\text{EIRP} = P_{\text{tx}} + G_{\text{ant}} \text{ (dBm + dBi)} \tag{19}$$

On-axis power density at range R:

$$S(R) = \frac{\text{EIRP}}{4\pi R^2} \text{ (W/m}^2\text{)} \tag{20}$$

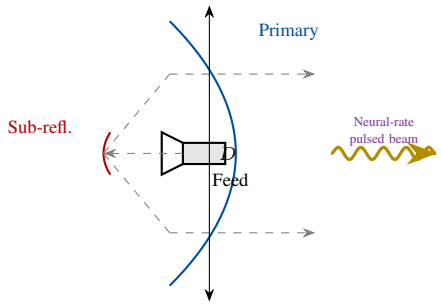

Fig. 9: Cassegrain reflector antenna producing a neural-rate pulsed sub-THz beam.

For pulsed operation, the *peak* power density during a pulse and the *average* power density differ by the duty cycle:

$$S_{\text{avg}} = \delta \cdot S_{\text{peak}} \tag{21}$$

This distinction is critical for neural-rate exposure analysis (Section XI).

IX. Complete System Architectures

A. Configuration 1: W-band Neural Pulser (102 GHz)

Key parameters:

- Carrier: 102 GHz; Peak power: 2 W
- Modulation: PIN switch (all three architectures)
- Antenna: Horn + 30 cm lens, 45 dBi
- EIRP: 78 dBm (CW equiv.), up to 82 dBm pulsed
- Neural PRF range: 0.5–100 Hz (all bands)
- Burst intra-rate: up to 50 kHz

B. Configuration 2: D/G-band High-Power Neural Pulser (153–204 GHz)

Key parameters:

- Carrier: 153 or 204 GHz; Peak power: 50–400 W
- Modulation: Grid-pulsed EIK (all architectures)
- Antenna: 50 cm Cassegrain, 53 dBi
- EIRP: 100–109 dBm (10–80 GW isotropic equiv.)
- Beamwidth: 0.3° pencil beam
- Neural PRF: 0.5–100 Hz; Burst rate: to 50 kHz

C. Configuration 3: Sub-THz Neural Pulser (306 GHz)

Key parameters:

- Carrier: 306 GHz; Peak power: 0.2–1 W
- Modulation: Grid-pulsed EIK
- Antenna: Horn + 20 cm Si lens, 50 dBi
- EIRP: 73–80 dBm
- Maximum atmospheric penetration at sea level limited; best suited for short-range (<100 m) or controlled environments

Configuration 1: W-band Neural Pulser

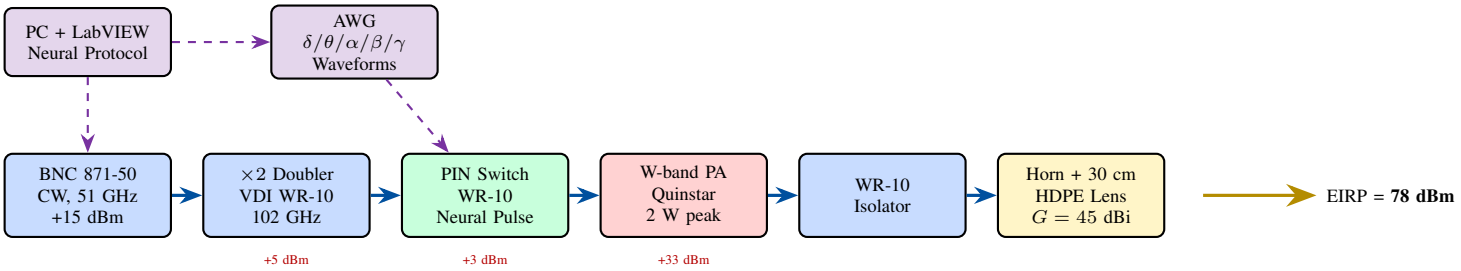

Fig. 10: Configuration 1: W-band (102 GHz), 2 W peak, solid-state PA, PIN-diode neural pulse modulation. EIRP = 78 dBm.

Configuration 2: D/G-band High-Power Neural Pulser

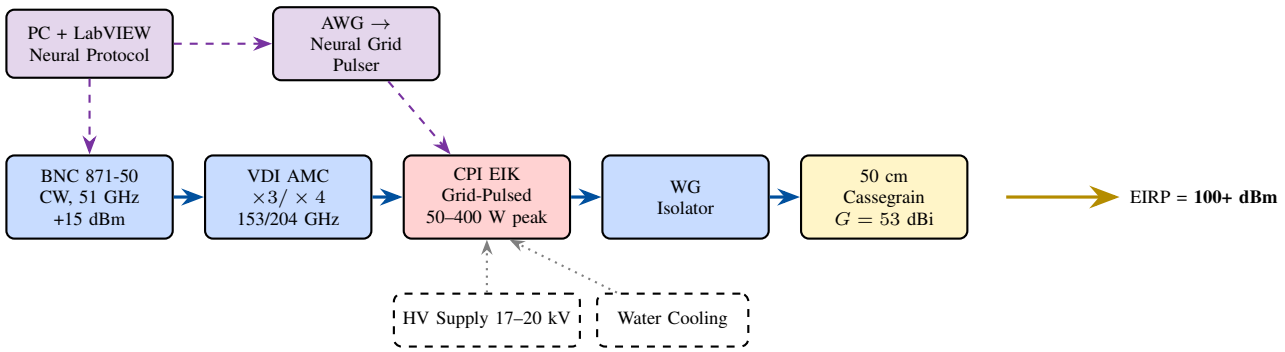

Fig. 11: Configuration 2: D/G-band (153–204 GHz), CPI EIK amplifier, grid-pulsed neural modulation, 50 cm Cassegrain (53 dBi). EIRP $>$ 100 dBm.

TABLE XIV: Complete System Configuration Comparison

Parameter	**Config. 1 (W-band)**	**Config. 2 (D/G)**	**Config. 3 (Sub-THz)**
Carrier frequency	102 GHz	153/204 GHz	306 GHz
Carrier wavelength	2.9 mm	2.0/1.5 mm	1.0 mm
Multiplication	×2	×3/×4	×6
PA technology	Solid-state MMIC	CPI EIK	CPI EIK
CW output power	2 W	5–20 W	0.1–0.2 W
Peak pulsed power	5 W	50–400 W	0.5–1 W
Neural modulation	PIN switch	Grid-pulsed EIK	Grid-pulsed EIK
Neural PRF range	0.5–100 Hz	0.5–100 Hz	0.5–100 Hz
Burst intra-rate	to 50 kHz	to 1 MHz	to 1 MHz
Antenna	Horn + 30 cm lens	50 cm Cassegrain	Horn + 20 cm Si lens
Gain	45 dBi	53 dBi	50 dBi
EIRP (peak)	78–82 dBm	100–109 dBm	73–80 dBm
Beamwidth	0.7°	0.3°	0.3°
Tissue pen. depth	∼0.3 mm	∼0.2 mm	∼0.1 mm
Complexity	Low	High	Very High
Cost estimate	$170k	$500k	$640k

D. Configuration Comparison

X. Man-Portable System Configuration

A critical operational requirement for many disruption scenarios is man-portability—the ability for a single operator to carry, deploy, aim, and operate the system without vehicle support. This section analyzes the size, weight, and power (SWaP) constraints and presents a field-deployable variant derived from Configuration 1.

A. SWaP Budget Analysis

Table XV decomposes the man-portable system into its constituent subsystems with estimated volume, mass, and DC power consumption.

B. Key Design Trades for Portability

1) Signal Source Miniaturization: The laboratory-grade BNC Model 871 (19-inch rack-mount, ∼15 kg) is replaced by a compact V-band phase-locked oscillator (PLO) module.

TABLE XV: Man-Portable SWaP Budget (W-band, 102 GHz)

Subsystem	Vol. (L)	Mass (kg)	DC (W)
V-band PLO module (compact)	0.8	1.2	15
×2 doubler (VDI)	0.05	0.08	—
W-band PA (GaN MMIC)	0.3	0.5	25
PIN switch + driver	0.1	0.15	2
AWG / pulse gen. (embedded)	0.2	0.3	5
Microcontroller + firmware	0.1	0.1	3
Horn + 15 cm HDPE lens	0.8	0.6	—
DC-DC converters	0.3	0.4	5 (overhead)
Battery (Li-ion, 28 V)	1.5	2.5	—
Enclosure + heatsink	1.0	1.5	—
Cabling, WG, misc.	0.3	0.4	—
Total	**5.5**	**7.7**	**55**

No commercial off-the-shelf bench synthesizer currently covers 51 GHz in a sub-liter form factor; however, custom V-band PLO modules employing a multiplied OCXO reference locked to a GaAs MMIC VCO at 51 GHz achieve $<$0.01 Hz resolution in volumes under 1 L and masses under 1.5 kg. The pulse modulation function is moved entirely to the external PIN switch, simplifying the source requirements to CW output only.

Alternatively, a fixed-frequency dielectric resonator oscillator (DRO) at 51 GHz with a voltage-controlled frequency trim ($\pm$50 MHz) can serve as an ultra-compact source ($<$50 cm^3, $<$200 g), trading frequency agility for extreme miniaturization. DROs at V-band are commercially available from vendors such as Microwave Dynamics and MACOM in compact hermetic packages.

2) Solid-State Power Amplification: The elimination of vacuum electronic devices (EIKs) is the single largest driver of portability. EIKs require 15–24 kV high-voltage supplies ($\sim$30 kg), water cooling loops ($\sim$10 kg), and filament power systems that collectively preclude man-portable deployment. Solid-state GaN MMIC PAs at W-band provide 1–5 W output power with DC-to-RF efficiency of 10–20%, operating from a 28 V DC bus compatible with standard military battery packs. Emerging GaN-on-SiC MMIC technology is projected to achieve 5–10 W at 94 GHz in chip-scale packages within the near term.

At 1 W output power with a 15 cm lens antenna (40 dBi gain), the man-portable system achieves:

$$\text{EIRP} = 30\ \text{dBm} + 40\ \text{dBi} = 70\ \text{dBm}\ (10\ \text{MW isotropic equiv.}) \tag{22}$$

3) Antenna Aperture vs. Gain Trade-off: Antenna diameter is the primary dimension driver. A 15 cm HDPE lens at 102 GHz provides:

$$G \approx \eta_{\text{sys}} \left(\frac{\pi \times 0.15}{0.0029} \right)^2 \approx 40\ \text{dBi} \quad (\eta_{\text{sys}} \approx 0.30) \tag{23}$$

$$\theta_{\text{3dB}} \approx 70 \times \frac{0.0029}{0.15} \approx 1.4^\circ \tag{24}$$

A 1.4° beamwidth illuminates a spot diameter of $\sim$2.4 m at 100 m range, sufficient for individual targeting at typical operational distances. Reducing the aperture to 10 cm ($G \approx 35$ dBi, $\theta_{\text{3dB}} \approx 2.0^\circ$) permits a more compact form factor at the cost of 5 dB EIRP and a 3.5 m spot at 100 m.

4) Battery Endurance: At 55 W total DC draw, a 28 V lithium-ion battery pack with 200 Wh capacity (standard military BB-2590/U form factor, 1.5 kg, 0.8 L) provides:

$$t_{\text{run}} = \frac{200\ \text{Wh}}{55\ \text{W}} \approx 3.6\ \text{hours continuous} \tag{25}$$

For pulsed neural disruption at low duty cycles (10% at alpha-band PRF), the PA operates at $\sim$10% average DC draw, extending effective endurance to $>$10 hours. A second battery (hot-swappable) provides mission-length autonomy.

C. Man-Portable Form Factors

Three man-portable configurations are feasible within the 7.7 kg SWaP budget:

1) Rifle-Style Configuration: The most operationally intuitive form factor arranges all subsystems along a single longitudinal axis, yielding a weapon-like profile ($\sim$60 cm × 20 cm × 15 cm, 7.5 kg loaded) comparable in size and weight to a compact carbine such as the M4.

Internal layout. The 15 cm HDPE plano-convex lens antenna occupies the forward aperture, recessed $\sim$5 mm behind an RF-transparent radome (HDPE or Rexolite, $<$0.3 dB insertion loss at W-band). Immediately behind the lens, the corrugated conical feed horn couples to a short section of WR-10 waveguide running aft through the central body. The waveguide path connects, in sequence, the VDI WR10x2 doubler, PIN diode switch, WR-10 isolator, and GaN MMIC PA module, all hard-mounted to a common aluminum chassis rail that doubles as the primary heatsink. The V-band PLO source module sits aft of the PA, with its coaxial output coupled to the doubler input via a coax-to-waveguide transition. The rear stock houses the embedded pulse-generator/microcontroller PCB, DC-DC converters, and the BB-2590/U battery pack, accessible through a hinged stock plate for field swap.

Thermal management. At 55 W total DC dissipation (dominated by the PA's $\sim$25 W), the chassis rail conducts heat to external longitudinal fins machined into the enclosure sidewalls. Natural convection in ambient conditions ($>$5°C) maintains the PA junction temperature below the GaN MMIC rated maximum ($T_j < 200$°C) without forced airflow. For sustained CW operation in high-ambient environments, a single 40 mm brushless fan ($<$30 g) mounted at the stock vent provides adequate margin.

Aiming and targeting. A Picatinny rail segment along the top surface accepts standard optical sights or a bore-sighted visible laser diode (Class 3R, 532 nm) co-aligned with the RF boresight to $<$0.5 mrad. Because the 1.4° RF beam illuminates

TABLE XVI: Man-Portable Form Factor Comparison

Form Factor	Dims. (cm)	Mass	Aperture	Gain	Deploy	Best Use Case
Rifle-style	60×20×15	7.5 kg	15 cm	40 dBi	<5 s	Overt rapid engagement, mobile operator, point-and-shoot
Backpack + gimbal	Pack: 30×20×15; Head: 20×20×15	8 kg	15 cm	40 dBi	30–60 s	Fixed-position overwatch, sustained exposure, stable aim
Briefcase (covert)	45×35×12	8 kg	10 cm	35 dBi	<5 s	Close-range clandestine, urban/permissive, attribution-resistant

a ∼2.4 m spot at 100 m, pointing precision of $\pm 0.5^\circ$ (readily achievable with a shoulder-braced stance) keeps the target within the -3 dB contour at ranges up to 75 m. A simple trigger switch on the pistol grip gates the PIN diode modulator, ensuring zero RF emission when not deliberately engaged.

Operational profile. This configuration is optimized for overt or semi-overt use by trained operators requiring rapid deployment, intuitive point-and-shoot targeting, and single-person carry. The weight and ergonomics are compatible with standard infantry load-bearing equipment and two-handed unsupported aim for engagements up to ∼60 seconds.

2) Backpack + Gimbal Head Configuration: This configuration separates the RF front-end from the electronics and power subsystems, distributing mass across the operator's torso and a lightweight tripod-mounted emitter head. Total system mass is ∼8 kg: 5.5 kg in the backpack unit and 2.5 kg in the gimbal head assembly.

Backpack unit. A standard MOLLE-compatible pack (30 cm × 20 cm × 15 cm external) houses the V-band PLO source, embedded pulse-generator/microcontroller, DC-DC converters, and two BB-2590/U batteries (series-connected for 28 V, ∼430 Wh total, providing >7 hours continuous or >20 hours pulsed endurance). A multi-conductor cable (∼2 m) and a flexible WR-10 waveguide section (or low-loss coaxial line at 51 GHz, with the doubler relocated to the head) connect the pack to the remote emitter head. The waveguide run introduces ∼1–2 dB additional insertion loss, partially offset by eliminating the need for a long high-frequency waveguide path.

Gimbal head. The emitter head (20 cm × 20 cm × 15 cm) contains the VDI doubler (if not in the pack), PIN switch, GaN MMIC PA, isolator, feed horn, and 15 cm HDPE lens in a sealed weatherproof housing. The head mounts on a lightweight carbon-fiber tripod via a manual pan-tilt gimbal with friction locks, providing stable aiming without operator fatigue. A coarse bore-sighted optical sight or red-dot optic on the head enables targeting. For extended surveillance-type missions, the tripod-mounted head can be left on station while the operator maintains standoff from the emitter position.

Operational profile. This configuration prioritizes sustained operation, stable aiming, and operator comfort over rapid deployment. The tripod eliminates pointing jitter entirely, making it well suited for fixed-position or overwatch scenarios where the operator can set up the head with 30–60 seconds of preparation time. The decoupled mass distribution (∼5.5 kg on back, ∼2.5 kg carried or tripod-mounted) substantially reduces operator fatigue for extended missions.

3) Briefcase Configuration (Covert): For clandestine deployment in permissive or urban environments, all components are integrated within a standard-appearance hard-shell attaché case (45 cm × 35 cm × 12 cm, ∼8 kg), visually indistinguishable from a commercial laptop case or equipment carrier.

Internal layout. The case interior is divided into two compartments by a horizontal bulkhead. The upper compartment (case lid) houses the flat-profile antenna assembly: a 10 cm HDPE lens bonded to the inner surface of an RF-transparent window panel (HDPE or PTFE, machined flush with the case exterior). The lens radiates through the case wall in the direction the lid faces when the case is held vertically at the operator's side, or in the direction the case is oriented when set on a surface. The lower compartment contains the RF chain (PLO, doubler, PIN switch, PA, isolator) mounted on an aluminum baseplate heatsink, the embedded pulse-generator, DC-DC converters, and a single BB-2590/U battery.

Antenna and beamwidth. The 10 cm aperture provides $G \approx 35$ dBi with a 2.0° beamwidth, illuminating a ∼3.5 m spot at 100 m. The wider beam relaxes pointing accuracy to $\pm 1.0^\circ$, which is achievable by gross orientation of the case body without fine aiming aids. At the cost of 5 dB EIRP relative to the 15 cm rifle-style configuration, the covert form factor trades maximum range for concealment.

Thermal management. The aluminum baseplate conducts PA heat to the case bottom surface, which acts as a distributed radiator. For intermittent operation (30 seconds on, 2 minutes off), surface temperature remains below 45°C. Sustained CW operation is thermally limited to ∼5 minutes before the PA requires a cooldown cycle, though neural-rate pulsed operation at 10% duty cycle extends this to >30 minutes.

Activation and control. A recessed membrane switch panel on the case handle or side provides mode selection (neural band, pulse architecture, power level) and a discrete activation button. An optional Bluetooth Low Energy link to a smartphone application permits remote arming and parameter adjustment, allowing the operator to position the case and control it from several meters away.

Operational profile. This configuration is designed for close-range engagements (<50 m) in environments where overt weapon-like devices are impermissible. The operator carries or positions the case in proximity to the target and activates remotely or via the handle controls. Effective use requires intelligence preparation to establish the target's expected position relative to the case orientation. The 10 cm

TABLE XVII: Man-Portable System Performance

Parameter	Value
Carrier frequency	102 GHz
Output power (peak)	1–2 W (GaN MMIC)
Antenna gain	35–40 dBi (10–15 cm lens)
EIRP (peak)	65–73 dBm
Beamwidth	1.4–2.0°
Beam spot at 100 m	2.4–3.5 m diameter
Neural PRF range	0.5–100 Hz
Pulse architectures	I, II, III (all supported)
Total mass	<8 kg (with battery)
Total volume	<6 L
Battery endurance	3.6 h CW / >10 h pulsed
Effective range	10–200 m (disruption)

aperture and lower EIRP make this the shortest-range variant, but its indistinguishable external appearance provides attribution resistance that the other form factors cannot match.

D. Man-Portable Performance Summary

The on-axis power density at range R for the man-portable system:

$$S(R) = \frac{P_{\text{pk}} \cdot G}{4\pi R^2} \tag{26}$$

At 1 W peak, 40 dBi gain:

- $S(10\text{ m}) = 7.96\text{ W/m}^2 = 0.80\text{ mW/cm}^2$ (exceeds lower-frequency effective threshold of 0.3 mW/cm^2 [12])
- $S(50\text{ m}) = 0.32\text{ W/m}^2 = 0.032\text{ mW/cm}^2$
- $S(100\text{ m}) = 0.080\text{ W/m}^2 = 0.008\text{ mW/cm}^2$

The sub-THz volumetric SAR advantage (Section III, Eq. 11) implies that these power densities—while lower than the 1–10 GHz effective thresholds—may produce comparable volumetric energy deposition in the absorption layer due to the 50× shallower penetration depth. At 10 m range, the power density is ∼3× above the scaled effective threshold, suggesting disruption efficacy within short-to-medium standoff distances.

E. Scaling to Higher Power

The man-portable SWaP budget can accommodate increased output power as GaN MMIC technology matures:

- **2 W GaN PA** (current state-of-art): +3 dB EIRP, doubling the effective range for equivalent disruption threshold.
- **5 W GaN PA** (near-term projection): +7 dB EIRP. DC power increases to ∼50 W (PA only), still within battery budget with reduced endurance (∼2 h continuous).
- **Power combining**: Two 2 W MMICs combined via a waveguide combiner provide 4 W with <0.5 dB combining loss, at the cost of ∼0.3 kg and 25 W additional DC.

For vehicle-mounted deployment (removing the mass constraint), a compact EIK-based system with 10 W output and 30 cm Cassegrain (45 dBi) achieves EIRP ≈ 85 dBm in a ∼50 kg package, providing disruption-effective power densities to 500+ m range.

TABLE XVIII: Electromagnetic Penetration Depth in Skin Tissue

Frequency (GHz)	δ_p (μm)	Primary Absorber
100	300–400	Water in dermis
150	200–300	Water in dermis
200	150–200	Water in epidermis
300	80–120	Water in stratum corneum

XI. Bioelectromagnetic Considerations

A. Tissue Interaction at Sub-THz Frequencies

At 100–300 GHz, electromagnetic radiation is absorbed primarily in the superficial layers of biological tissue (skin, cornea) due to the high water content absorption. The penetration depth δ_p is:

$$\delta_p = \frac{1}{2\alpha} = \frac{c}{4\pi f \cdot \text{Im}(\sqrt{\epsilon_r})} \tag{27}$$

B. Neural Relevance of Pulsed Sub-THz Exposure

The efficacy of sub-THz neural disruption depends on the coupling efficiency between incident pulsed radiation and the neural circuits governing vestibular, cognitive, and autonomic function. The neurophysiological basis established in Section III identifies the specific disruption pathways; this section quantifies the biophysical coupling mechanisms that determine the dose–response relationship for each disruption modality.

1) Thermal Pulsing and Thermoreceptor Entrainment: Each sub-THz pulse deposits energy in superficial tissue, creating a microscopic temperature transient. At neural PRFs, this creates a periodic temperature modulation at the tissue surface:

$$\Delta T(t) = \frac{S_{\text{peak}} \cdot \tau_p}{\rho c_p \cdot \delta_p} \cdot h(t) * p(t) \tag{28}$$

where $h(t)$ is the thermal impulse response and $p(t)$ is the neural pulse train. The thermal time constant of skin (∼1 s) provides significant temporal averaging, but at low duty cycles the peak temperature rise per pulse may be detectable by thermoreceptors.

For Configuration 2 at 153 GHz with alpha-band pulsing (10 Hz, 10% duty cycle, 10 W peak power), the per-pulse temperature rise at the skin surface at 10 m range is estimated as:

$$\Delta T_{\text{pulse}} \approx \frac{S_{\text{peak}} \cdot \tau_p}{\rho c_p \cdot \delta_p} \approx \frac{158 \times 0.01}{1000 \times 3500 \times 2 \times 10^{-4}} \approx 0.023\ ^\circ\text{C} \tag{29}$$

Transient receptor potential (TRP) channels—specifically TRPV1 and TRPV3—can detect temperature changes as small as 0.003°C when these changes are presented as temporal gradients rather than steady-state shifts [28]. The rapid onset ($\sim \mu$s thermal diffusion time through the absorption depth) and periodic nature of the sub-THz thermal pulses may therefore produce a detectable, entrained thermoreceptor signal at the PRF frequency.

2) Peripheral Nerve Activation and Disruption Signal Propagation: Free nerve endings in the epidermis and dermis respond to thermal gradients. Periodic sub-THz pulses at neural frequencies entrain firing patterns in peripheral sensory neurons, which propagate to central neural circuits via thalamocortical pathways. The disruption signal path follows a well-characterized afferent cascade:

1) **Transduction**: Thermoreceptive C-fibers and Aδ-fibers in the superficial skin layers detect pulsed thermal transients at the PRF frequency.
2) **Spinal relay**: Signals propagate via the dorsal root ganglia to the spinothalamic tract.
3) **Thalamic entrainment**: The VPL nucleus of the thalamus receives the periodic afferent input. Because this nucleus shares reciprocal connections with the thalamic reticular nucleus (the alpha rhythm pacemaker), the periodic input directly perturbs the endogenous oscillatory machinery.
4) **Cortical disruption**: Thalamocortical projections deliver the externally forced oscillation to somatosensory cortex (S1), motor cortex (M1), and vestibular cortex, disrupting the endogenous rhythms that maintain sensorimotor integration and spatial orientation.
5) **Vestibular cascade**: Via vestibulothalamic reciprocal connections, the entrained thalamic oscillation propagates to the vestibular nuclei, creating the sensory conflict that triggers nausea and vertigo (Section III).

The latency from skin irradiation to cortical disruption onset is estimated at 50–200 ms (afferent conduction + thalamic relay + cortical processing). Sustained exposure at the appropriate PRF produces progressive entrainment, with the discombobulating effect building over 10–60 s as the endogenous oscillation locks to the external driving frequency.

3) Direct Field Effects on Neural Substrates: At the quantum mechanical level, sub-THz photon energies ($h\nu \approx 0.4$–1.2 meV at 100–300 GHz) are far below thermal energy ($k_B T \approx 26$ meV at body temperature). However, several non-thermal interaction mechanisms remain under active investigation [8], [9]:

- **Protein conformational dynamics**: Many protein vibrational modes (particularly collective backbone motions) have resonance frequencies in the 0.1–1 THz range. Pulsed sub-THz radiation may selectively excite these modes [29].
- **Water network perturbation**: The relaxation dynamics of interfacial water surrounding membrane proteins occur on picosecond timescales corresponding to sub-THz frequencies. Periodic perturbation of the hydration shell could modulate protein function.
- **Ion channel gating**: Voltage-gated ion channels undergo conformational transitions involving charge movement across the membrane. Whether sub-THz fields can couple to these gating transitions—even at sub-thermal photon energies—remains an open question of considerable significance.

4) The Thermoelastic Hypothesis: At lower carrier frequencies (1–3 GHz), pulsed EM radiation produces thermoelastic expansion of tissue, generating acoustic pressure waves within the head [10], [16]. While the sub-THz carrier frequencies employed by the present system are absorbed in the superficial skin layers (not within the cranium), the thermoelastic mechanism remains relevant for the skin itself: rapid pulsed heating produces microscale mechanical stress waves that may activate mechanosensitive ion channels (Piezo1, Piezo2) in cutaneous nerve endings, providing an additional transduction pathway beyond pure thermoreception.

TABLE XIX: Pulsed vs. CW Exposure Comparison (Config. 2, 153 GHz, 5 W CW rating)

Parameter	**CW**	**α pulse 10 Hz, 10%**	**δ pulse 2 Hz, 5%**
Peak power	5 W	10 W	20 W
Avg. power	5 W	1 W	1 W
S_{peak} at 10 m	79 W/m^2	158 W/m^2	316 W/m^2
S_{avg} at 10 m	79 W/m^2	15.8 W/m^2	15.8 W/m^2

TABLE XX: Free-Space Path Loss at Target Frequencies

Range	**102 GHz**	**153 GHz**	**306 GHz**
1 m	62 dB	66 dB	72 dB
10 m	82 dB	86 dB	92 dB
100 m	102 dB	106 dB	112 dB

C. Pulsed vs. CW Exposure Considerations

The neural-rate pulsing fundamentally changes the exposure profile compared to CW:

The distinction between peak and average power density is critical. While average exposure may be below MPE limits, peak pulse power density can be 10–20$\times$ higher than CW, creating transient thermal gradients that may have biological significance distinct from average heating.

XII. Beam Propagation and Link Analysis

A. Free-Space Path Loss

$$\text{FSPL} = 20 \log_{10} \left(\frac{4\pi R}{\lambda} \right) \text{ dB} \tag{30}$$

B. Atmospheric Attenuation

For indoor laboratory distances (<50 m), atmospheric attenuation is negligible (<0.5 dB). For outdoor propagation, sea-level attenuation ranges from 0.4 dB/km (100 GHz) to 5 dB/km (300 GHz).

C. Neural Pulse Received Power Temporal Profile

At the target, the received power exhibits the neural pulse temporal structure:

$$P_r(t) = \frac{P_t(t) \cdot G_t \cdot A_r}{(4\pi R)^2} \tag{31}$$

where $P_t(t)$ contains the neural-rate modulation. The received signal faithfully reproduces the transmitted pulse architecture (I, II, or III), with the temporal structure preserved exactly (propagation delay is $R/c \approx 33$ ns at 10 m, negligible compared to neural periods).

TABLE XXI: Maximum Permissible Exposure (MPE) Limits

Standard	Category	MPE	Avg.
ICNIRP 2020	Occupational	5 mW/cm^2	6 min
	General public	1 mW/cm^2	30 min
IEEE C95.1	Controlled	5 mW/cm^2	6 min
	Uncontrolled	1 mW/cm^2	30 min

TABLE XXII: Conservative Hazard Distances (Peak Power Basis)

Config.	P_{pk}	R_{haz} (occ.)	R_{haz} (pub.)
1 (102 GHz)	5 W, 45 dBi	89 m	199 m
2 (153 GHz)	20 W, 53 dBi	502 m	1.1 km
3 (306 GHz)	1 W, 50 dBi	126 m	282 m

XIII. Safety Protocols and Regulatory Compliance

A. RF Exposure Limits

B. Pulsed Exposure Assessment

Current MPE standards are based on *average* power density over the specified averaging time. For neural-rate pulsed systems, the average power density is:

$$S_{\text{avg}} = \delta \cdot S_{\text{peak}} \tag{32}$$

However, there is ongoing scientific debate regarding whether peak pulse power density or specific temporal modulation patterns may have effects not captured by average-power-based limits [11]. **Conservatively, this system should be treated as if peak power density applies for safety calculations.**

C. Hazard Distance Calculation

Using *peak* power for conservative safety:

$$R_{\text{haz}} = \sqrt{\frac{P_{\text{peak}} \cdot G}{4\pi \cdot S_{\text{MPE}}}} \tag{33}$$

D. Mandatory Safety Measures

1) **Controlled access**: Interlocked enclosure encompassing the full beam path to R_{haz}.
2) **RF absorber termination**: Beam terminates on rated mmW absorber (Eccosorb AN/TK RAM).
3) **Class 4 laser equivalence**: Treat as Class 4 laser hazard—engineering controls, key switch, emergency stop, warning indicators.
4) **Interlock chain**: Door $\rightarrow$ relay $\rightarrow$ EIK HV crowbar / PA disable / PIN switch open. Failsafe (de-energize on break).
5) **HV electrical safety**: 17–24 kV EIK supplies present **lethal electrocution hazard**. Interlocked HV enclosures, stored-energy discharge protocol, qualified personnel only.
6) **Signage**: IEEE/ANSI RF hazard signs at all access points.
7) **Training**: All personnel: RF safety + HV safety certification.
8) **Institutional review**:
   - EHS approval before system energization.
   - **IRB approval required** if any experiment involves human subjects, tissue samples, or animal models.
   - Radiation Safety Committee review.
9) **Neural-specific protocols**: Given the deliberate targeting of neural oscillation frequencies, additional precautionary measures:
   - Document all pulse parameters for every experiment.
   - Real-time power monitoring with automatic shutdown if power exceeds setpoint.
   - Exposure duration limits per session.
   - Exclusion zones enforced during neural-rate pulsed operation.

XIV. Budget Estimates

XV. Integration and Neural Protocol Testing

A. Phase 1: RF Chain Verification

1) Verify BNC 871 at 51 GHz: power, spectral purity.
2) Characterize multiplier output at target frequency.
3) Verify PA gain, saturation, thermal stability.

B. Phase 2: Neural Pulse Modulation Verification

1) Program AWG with all five neural band waveforms (Table I).
2) Verify pulse timing with oscilloscope at modulator output:
   - Architecture I: Confirm PRF accuracy $<0.1\%$ at each neural band center frequency.
   - Architecture II: Verify envelope waveform fidelity using detected RF envelope vs. AWG reference.
   - Architecture III: Verify T_4, T_5, T_6 timing for each burst configuration (Table III).
3) Measure on/off extinction ratio at neural PRFs.
4) Characterize pulse rise/fall times; verify $\tau_{\text{rise}} < T_4/10$ for burst mode.
5) Record time-domain power envelope at multiple neural PRFs using fast power detector + oscilloscope.

C. Phase 3: Antenna and Beam Characterization

1) Antenna pattern measurement (gain, beamwidth, sidelobes).
2) EIRP verification at calibrated range.
3) Beam alignment and pointing accuracy.

D. Phase 4: Full System Neural Protocol Test

1) End-to-end test: AWG neural waveform $\rightarrow$ radiated pulsed beam.
2) Verify received pulse structure at target distance using calibrated detector.
3) Confirm all five neural band PRFs produce correct temporal structure.
4) Burst-mode verification: confirm T_4, T_5, T_6 at target.
5) Automated neural band sweep: $\delta \rightarrow \theta \rightarrow \alpha \rightarrow \beta \rightarrow \gamma$ in programmed sequence.

TABLE XXIII: Estimated Budget (USD, Approximate)

Category	Component	Config. 1	Config. 2	Config. 3
Signal Source	BNC 871-50 w/ MOD option	$60,000	$60,000	$60,000
Multiplier	VDI/Eravant chain	$15,000	$35,000	$55,000
PIN Modulator	Eravant WG switch + driver	$10,000	$5,000*	$5,000*
PA (Solid-State)	Quinstar W-band	$25,000	—	—
PA (VED)	CPI EIK + grid pulser	—	$200,000	$300,000
HV Power Supply	CPI PS-series	—	$50,000	$50,000
Cooling	Closed-loop chiller	—	$10,000	$10,000
Neural AWG	Keysight 33600A + PC	$12,000	$12,000	$12,000
LabVIEW + NI DAQ	Software + hardware	$8,000	$8,000	$8,000
Waveguide	Isolators, transitions	$5,000	$10,000	$15,000
Antenna (Feed)	Corrugated horn	$3,000	$5,000	$8,000
Antenna (Main)	Lens / Cassegrain	$8,000	$25,000	$15,000
Positioning	Gimbal + rotation stage	$5,000	$10,000	$10,000
Safety	Absorber, interlocks, signs	$5,000	$15,000	$15,000
Diagnostics	Power meter, spectrum analyzer	$15,000	$15,000	$15,000
Subtotal		**$171,000**	**$460,000**	**$578,000**
Contingency (15%)		$26,000	$69,000	$87,000
Total Estimate		**$197,000**	**$529,000**	**$665,000**

*Optional backup modulator in addition to EIK grid pulsing.

TABLE XXIV: Disruption-Optimized Protocol Library

Protocol	Arch.	PRF/Params	Dur.	Target Effect
α-Nausea	I	10 Hz, 30%	60 s	Vestibular nausea
α-Sweep	I	8–12 Hz sweep, 2 s/cycle	60 s	Broadband vestib. disruption
β-Motor	I	15 Hz, 20%	60 s	Motor impairment
β-Cognitive	I	18 Hz, 20%	90 s	Cognitive degrad.
β-Anxiety	I	25 Hz, 25%	120 s	Acute anxiety/panic
α+β compound	II	10 Hz + 20 Hz nested	120 s	Compound discombob.
Burst-Vestib.	III	10 Hz burst, 300 Hz intra	90 s	Max. vestibular crisis
Full-Spectrum	I	$\alpha \rightarrow \beta$ sweep, 5 s/step	300 s	Progressive escalation

6) Safety system verification: interlock testing, emergency shutdown latency.
7) Power density measurement at multiple ranges vs. MPE limits.

E. Phase 5: Neural Protocol Library

The following disruption-optimized protocol library provides pre-programmed waveforms targeting specific discombobulation modalities:

XVI. Discussion

A. Carrier Frequency Selection for Disruption Optimization

The choice of 100–300 GHz carrier frequencies represents an optimal trade-off between disruption efficacy, system portability, and attribution resistance. The sub-THz neural disruption approach differs fundamentally from existing directed-energy and neuromodulation technologies:

- **Transcranial magnetic stimulation (TMS)**: Uses single pulses or repetitive pulses at neural rates (rTMS), but the magnetic field directly induces currents in cortical tissue. TMS requires close proximity (<few cm) and uses frequencies below 100 Hz for the *carrier* (the stimulating pulse itself).
- **Transcranial alternating current stimulation (tACS)**: Applies weak AC currents at neural frequencies through scalp electrodes. Requires physical contact.
- **Microwave auditory effect (Frey effect)** [10]: Pulsed microwave radiation (0.2–3 GHz) at low PRFs creates thermoelastic expansion in the head, producing perceived sounds. The present system operates at much higher carrier frequencies with correspondingly shorter penetration depth.
- **Focused ultrasound neuromodulation**: Mechanical waves focused through skull to deep brain targets. Different physical interaction mechanism.

The sub-THz neural disruption system uniquely combines attributes that no existing technology provides:

1) **Standoff delivery**: Non-contact, directional operation at ranges of 10–500+ m
2) **Individual targeting**: Sub-degree beamwidth enables isolation of a single subject in a crowd
3) **Disruption specificity**: PRF selection determines *which* neurological function (vestibular, motor, cognitive) is degraded
4) **Escalation control**: Continuous PRF and power adjustment from subliminal to incapacitating
5) **Attribution resistance**: No visible beam, no audible signature; effects (nausea, vertigo, confusion) mimic common illness and leave no forensic trace
6) **Reversibility**: Effects cease within seconds to minutes after exposure termination, with no permanent injury at design power levels

B. Comparison with Lower-Frequency EM Approaches

The present sub-THz system (100–300 GHz) differs fundamentally from lower-frequency pulsed EM systems operating

TABLE XXV: Sub-THz vs. Lower-Frequency EM Neural-Rate Systems

Parameter	1–10 GHz	100–300 GHz
Pen. depth	3–20 mm	0.1–0.4 mm
Skull penetration	Partial	None
Primary coupling	Volumetric heating, thermoelastic	Surface thermal
Frey effect	Yes (at ∼1.3 GHz)	No
Antenna size for 0.5° beam	>1 m	<30 cm
Spatial precision	Low (cm-scale)	High (mm-scale)
Peak SAR	Distributed	Concentrated
Wall/window penetration	Good	Limited

in the 1–10 GHz range [12], [10]. Table XXV summarizes the key trade-offs.

For disruption applications, the sub-THz approach offers decisive operational advantages despite its shallower penetration depth. The indirect afferent pathway (thermoreceptor → thalamus → cortex → vestibular nuclei) is not a limitation but an advantage: it recruits the *endogenous* thalamocortical oscillatory machinery as an amplifier, allowing relatively weak peripheral stimuli to produce large-scale cortical and vestibular disruption through the entrainment mechanism (Section III). The compact antenna size (<30 cm for sub-degree beams) enables portable, concealable deployment configurations impossible at lower frequencies.

Lower-frequency systems (1–10 GHz) retain advantages for certain scenarios: they penetrate common building materials (walls, windows, doors), enabling through-wall operation [12], and can induce the Frey auditory effect (an additional disorientation vector). However, their large antenna requirements (>1 m for comparable directionality) and lower spatial precision (cm-scale beam cross-section) make them unsuitable for individual targeting in complex environments. A **hybrid architecture**—combining a sub-THz system for precision individual targeting with a lower-frequency (1–10 GHz) wide-beam system for area-effect disruption—would maximize operational flexibility.

C. Multi-Modal Stimulation Paradigm

The dual-modality approach described by Norris and Putterman—combining pulsed EM and pulsed ultrasonic waveforms at the same neural PRF—suggests a broader principle: multi-modal, phase-synchronized stimulation may achieve neural entrainment effects that single-modality approaches cannot [12], [27].

The present sub-THz system could serve as the EM component of such a dual-modality configuration. The ultrasonic component would operate at a carrier frequency of 40–50 kHz (above audibility threshold), amplitude-modulated at the same neural PRF. The phase relationship between the two modalities would be controlled by the unified LabVIEW system, with the ultrasonic waveform advanced by $\Delta t_{\text{latency}} \approx$ 10–50 ms relative to the EM waveform to achieve temporal coincidence at the cortical level.

The choice of ultrasonic carrier frequency involves a design trade-off: lower frequencies (∼40 kHz) provide greater range but may generate audible subharmonics (∼13 kHz), while higher frequencies (∼42–50 kHz) push the subharmonics above the audible range for most subjects at the cost of reduced propagation distance [12]. For laboratory configurations with short target distances (<10 m), carrier frequencies of 45–50 kHz are recommended.

D. Disruption Optimization Parameters

The following parameters determine disruption efficacy and should be characterized through systematic testing:

1) **Onset time vs. PRF**: How rapidly do discombobulating effects (nausea, vertigo, confusion) develop as a function of PRF within the alpha and beta bands? The 10 Hz alpha frequency is expected to produce the fastest vestibular disruption onset based on prior art [12], [17].
2) **Architecture efficacy ranking**: Does burst-mode pulsing (Architecture III), which replicates pathological thalamocortical discharge patterns, produce faster or more severe disruption than simple periodic pulsing (Architecture I)?
3) **Power density threshold**: What is the minimum incident power density at which disruption effects become detectable via the peripheral afferent pathway at sub-THz frequencies? How does this compare to the ∼0.3 mW/cm^2 threshold reported at 1–10 GHz [12]?
4) **Dual-modality enhancement factor**: What is the synergistic gain (reduction in onset time or required power density) when pulsed ultrasonic stimulation is added, and what inter-modality phase offset maximizes this gain?
5) **Beta sub-band selectivity**: Can low-beta motor impairment, mid-beta cognitive degradation, and high-beta anxiety induction be independently controlled through precision PRF selection?
6) **Frequency sweep vs. fixed PRF**: Does the frequency sweep strategy (Section III) reduce the onset time by ensuring rapid capture of the individual's endogenous oscillation frequency?
7) **Habituation and adaptation**: Do disruption effects diminish with prolonged or repeated exposure, and can Architecture switching (I → III → II) counteract adaptation?
8) **Carrier frequency dependence**: Does the concentrated surface absorption at 200–300 GHz produce stronger per-unit-power disruption than the distributed volumetric absorption at 100 GHz, as predicted by the volumetric SAR analysis (Section III)?

E. Operational Limitations

- **Line-of-sight requirement**: Sub-THz radiation does not penetrate common building materials (walls, glass, doors). Operation is limited to line-of-sight geometries. Through-wall operation requires a lower-frequency (<10 GHz) subsystem.
- **Indirect coupling pathway**: All neural disruption effects are mediated through the peripheral afferent pathway (thermal → thermoreceptor → afferent nerve → thalamic relay → cortical disruption), introducing 50–200 ms latency and potential signal attenuation. This limits the

maximum disruption forcing rate to the thalamocortical entrainment bandwidth.

- **Individual variability**: Endogenous oscillation frequencies vary ± 2 Hz (alpha) to ± 5 Hz (beta) across individuals. Fixed-frequency protocols will not achieve optimal disruption for all subjects. The frequency sweep strategy mitigates but does not eliminate this limitation.
- **Atmospheric attenuation**: At 300 GHz, sea-level attenuation of $\sim$5 dB/km limits outdoor range. Frequencies near 100 GHz (0.4 dB/km) are preferred for extended-range deployment.
- **Clothing and hair attenuation**: While sub-THz radiation penetrates light clothing and hair with modest attenuation (1–5 dB), heavy winter clothing or metallic-fiber fabrics provide significant shielding.

XVII. Conclusion

This paper has presented the complete engineering design of a directed sub-terahertz neural disruption system optimized for producing vestibular disorientation, nausea, cognitive degradation, and autonomic disturbance in targeted subjects at standoff range. The system exploits the fundamental vulnerability of thalamocortical oscillatory circuits to external entrainment, mapping disruption-relevant neural frequency bands onto three pulse architectures:

Architecture I (Continuous Pulse Train) provides sustained neural rhythm disruption at a selected target frequency, producing frequency-specific effects (alpha: vestibular nausea; beta: cognitive/motor degradation) with the simplest implementation.

Architecture II (Neural Waveform Envelope) maximizes entrainment efficacy by reproducing the complex morphology of endogenous neural oscillations, including cross-frequency coupling dynamics that compound multi-system disruption (simultaneous vestibular, cognitive, and motor degradation).

Architecture III (Burst-Mode Pulsing) replicates pathological thalamocortical discharge patterns to force the target's neural oscillatory circuits into states associated with absence seizure and vestibular crisis phenomenology, producing the most severe discombobulation.

Three laboratory configurations (102–306 GHz, 0.2–20 W peak, 73–96 dBm EIRP) and a man-portable variant (102 GHz, 1–2 W, $<$8 kg, $<$6 L) have been detailed with complete component specifications. The man-portable system achieves disruption-effective power densities at 10–200 m range in rifle-style, backpack, or covert briefcase form factors, demonstrating that neural-rate pulsed sub-THz directed energy is feasible as a field-deployable, individually targeted disruption capability.

The neurophysiological analysis identifies the specific vulnerabilities exploited by each disruption modality: thalamocortical pacemaker entrainment for vestibular disruption, beta sub-band selectivity for differential motor vs. cognitive degradation, and multi-modal (EM + ultrasonic) synergistic enhancement for compounded discombobulation. The frequency sweep strategy addresses individual variability in endogenous oscillation frequencies, ensuring broad-population efficacy.

Configuration 1 / man-portable (W-band, solid-state) is recommended as the primary deployment platform due to its portability, all-solid-state reliability, and sufficient EIRP for short-to-medium range disruption. Configuration 2 (D/G-band EIK) provides maximum power for extended-range or through-clothing scenarios requiring higher power density margins.

References

[1] G. Buzsáki, *Rhythms of the Brain*. Oxford University Press, 2006.

[2] L. M. Ward, "Synchronous neural oscillations and cognitive processes," *Trends Cogn. Sci.*, vol. 7, no. 12, pp. 553–559, 2003.

[3] C. M. Cook *et al.*, "Pulsed magnetic fields and cognition: An update," *Neurosci. Lett.*, vol. 407, no. 2, pp. 211–214, 2006.

[4] C. D. Hountala *et al.*, "Bioeffects of pulsed electromagnetic fields on brain electrical activity," *Arch. Environ. Health*, vol. 58, no. 8, pp. 503–508, 2008.

[5] R. T. Canolty and R. T. Knight, "The functional role of cross-frequency coupling," *Trends Cogn. Sci.*, vol. 14, no. 11, pp. 506–515, 2010.

[6] S. M. Sherman, "Tonic and burst firing: Dual modes of thalamocortical relay," *Trends Neurosci.*, vol. 24, no. 2, pp. 122–126, 2001.

[7] M. Steriade, D. A. McCormick, and T. J. Sejnowski, "Thalamocortical oscillations in the sleeping and aroused brain," *Science*, vol. 262, no. 5134, pp. 679–685, 1993.

[8] L. V. Titova *et al.*, "Intense THz pulses cause H2AX phosphorylation and activate DNA damage response in human skin tissue," *Biomed. Opt. Express*, vol. 4, no. 4, pp. 559–568, 2013.

[9] V. F. Kirichuk and A. N. Ivanov, "Regulatory effects of terahertz electromagnetic radiation," *J. Opt. Technol.*, vol. 78, no. 10, pp. 654–659, 2011.

[10] A. H. Frey, "Human auditory system response to modulated electromagnetic energy," *J. Appl. Physiol.*, vol. 17, no. 4, pp. 689–692, 1962.

[11] A. G. Pakhomov *et al.*, "Current state and implications of research on biological effects of millimeter waves," *Bioelectromagnetics*, vol. 19, no. 7, pp. 393–413, 1998.

[12] E. G. Norris and S. Putterman, "Systems and methods for covertly creating adverse health effects in subjects," U.S. Patent 11 801 394 B1, Oct. 31, 2023.

[13] F. H. Lopes da Silva, A. Hoeks, H. Smits, and L. H. Zetterberg, "Model of brain rhythmic activity: The alpha-rhythm of the thalamus," *Kybernetik*, vol. 15, no. 1, pp. 27–37, 1974.

[14] A. K. Engel and P. Fries, "Beta-band oscillations—signalling the status quo?," *Curr. Opin. Neurobiol.*, vol. 20, no. 2, pp. 156–165, 2010.

[15] B. E. Kilavik, M. Zaepffel, A. Brovelli, W. A. MacKay, and A. Riehle, "The ups and downs of beta oscillations in sensorimotor cortex," *Exp. Neurol.*, vol. 245, pp. 15–26, 2013.

[16] J. C. Lin and Z. Wang, "Hearing of microwave pulses by humans and animals: Effects, mechanism, and thresholds," *Health Phys.*, vol. 92, no. 6, pp. 621–628, 2007.

[17] J. G. Bovill, "The bucha effect: Adverse reactions to strobe illumination," *Aviat., Space, Environ. Med.*, vol. 49, pp. 1116–1118, 1978.

[18] R. S. Fisher *et al.*, "Photic- and pattern-induced seizures: A review for the Epilepsy Foundation of America Working Group," *Epilepsia*, vol. 46, no. 9, pp. 1426–1441, 2005.

[19] G. Buzsáki and X.-J. Wang, "Mechanisms of gamma oscillations," *Annu. Rev. Neurosci.*, vol. 35, pp. 203–225, 2012.

[20] J. A. Cardin *et al.*, "Driving fast-spiking cells induces gamma rhythm and controls sensory responses," *Nature*, vol. 459, no. 7247, pp. 663–667, 2009.

[21] G. Thut, P. G. Schyns, and J. Gross, "Entrainment of perceptually relevant brain oscillations by non-invasive rhythmic stimulation of the human brain," *Front. Psychol.*, vol. 2, art. 170, 2011.

[22] C. S. Herrmann, D. Strüber, R. F. Helfrich, and A. K. Engel, "EEG oscillations: From correlation to causality," *Int. J. Psychophysiol.*, vol. 103, pp. 12–21, 2016.

[23] A. Pikovsky, M. Rosenblum, and J. Kurths, *Synchronization: A Universal Concept in Nonlinear Sciences*. Cambridge University Press, 2001.

[24] P. Lakatos, G. Karmos, A. D. Mehta, I. Ulbert, and C. E. Schroeder, "Entrainment of neuronal oscillations as a mechanism of attentional selection," *Science*, vol. 320, no. 5872, pp. 110–113, 2008.

[25] K. E. Mathewson, G. Gratton, M. Fabiani, D. M. Beck, and T. Ro, "To see or not to see: Prestimulus alpha phase predicts visual awareness," *J. Neurosci.*, vol. 29, no. 9, pp. 2725–2732, 2009.

TABLE XXVI: Rectangular Waveguide Standards

WG	**Band**	$a \times b$ **(mm)**	**Range**	**Flange**
WR-10	W	2.54×1.27	75–110	UG-387
WR-6.5	D	1.65×0.83	110–170	UG-387/UM
WR-5.1	G	1.30×0.65	140–220	UG-387/UM
WR-3.4	Y	0.86×0.43	220–330	UG-387/UM

TABLE XXVII: Quick Reference: Neural Band $\rightarrow$ Pulse Parameters (Architecture I, $\delta = 10\%$)

Band	f	τ_p	Δt
δ (0.5 Hz)	0.5 Hz	200 ms	1.8 s
δ (4 Hz)	4 Hz	25 ms	225 ms
θ (6 Hz)	6 Hz	16.7 ms	150 ms
α (10 Hz)	10 Hz	10 ms	90 ms
α (13 Hz)	13 Hz	7.7 ms	69 ms
β (20 Hz)	20 Hz	5 ms	45 ms
β (30 Hz)	30 Hz	3.3 ms	30 ms
γ (40 Hz)	40 Hz	2.5 ms	22.5 ms
γ (60 Hz)	60 Hz	1.67 ms	15 ms
γ (100 Hz)	100 Hz	1 ms	9 ms

[26] T. H. Grandy, M. Werkle-Bergner, Y. L. Chicherio, F. Schmiedek, M. Lövdén, and U. Lindenberger, "Peak individual alpha frequency qualifies as a stable neurophysiological trait marker in healthy younger and older adults," *Psychophysiology*, vol. 50, no. 6, pp. 570–582, 2013.

[27] P. Lakatos, C.-M. Chen, M. N. O'Connell, A. Mills, and C. E. Schroeder, "Neuronal oscillations and multisensory interaction in primary auditory cortex," *Neuron*, vol. 53, no. 2, pp. 279–292, 2007.

[28] J. Vriens, B. Nilius, and T. Voets, "Peripheral thermosensation in mammals," *Nat. Rev. Neurosci.*, vol. 15, no. 9, pp. 573–589, 2014.

[29] A. G. Markelz, "Terahertz dielectric sensitivity to biomolecular structure and function," *IEEE J. Sel. Top. Quantum Electron.*, vol. 14, no. 1, pp. 180–190, 2008.

[30] C. Lopez and O. Blanke, "The thalamocortical vestibular system in animals and humans," *Brain Res. Rev.*, vol. 67, no. 1–2, pp. 119–146, 2012.

[31] J. T. Reason and J. J. Brand, *Motion Sickness*. Academic Press, 1975.

[32] B. J. Yates, A. D. Bolton, and D. M. Macefield, "Vestibulo-sympathetic responses," *Compr. Physiol.*, vol. 4, no. 2, pp. 851–887, 2014.

[33] P. H. Siegel, "Terahertz technology," *IEEE Trans. Microw. Theory Techn.*, vol. 50, no. 3, pp. 910–928, 2002.

[34] J. H. Booske *et al.*, "Vacuum electronic high power terahertz sources," *IEEE Trans. THz Sci. Technol.*, vol. 1, no. 1, pp. 54–75, 2011.

[35] ICNIRP, "Guidelines for limiting exposure to electromagnetic fields (100 kHz to 300 GHz)," *Health Phys.*, vol. 118, no. 5, pp. 483–524, 2020.

[36] IEEE, "IEEE Std C95.1-2019: Safety levels with respect to human exposure to EMF, 0 Hz to 300 GHz," 2019.

[37] N. S. DeLisio and R. A. York, "Quasi-optical and spatial power combining," *IEEE Trans. Microw. Theory Techn.*, vol. 50, no. 3, pp. 929–936, 2002.

Appendix A
Waveguide and Flange Standards

Appendix B
Neural Oscillation Pulse Timing Quick Reference

Appendix C
Phase Noise Budget

The phase noise at neural-rate offsets (0.5–100 Hz) is most critical for determining spectral purity of the pulse-modulated signal. The BNC 871's OCXO reference provides excellent close-in performance, ensuring clean spectral lines at neural PRFs even after $\times 6$ multiplication.

TABLE XXVIII: Phase Noise Budget at 10 kHz Offset (dBc/Hz)

Stage	$\times 2$	$\times 3$	$\times 6$
BNC 871 @ 51 GHz	-95	-95	-95
Mult. degradation	+6.0	+9.5	+15.6
Additive noise	+3	+4	+6
Total	$\mathbf{-86}$	$\mathbf{-81.5}$	$\mathbf{-73.4}$

Appendix D
Gaussian Beam Propagation

For quasi-optical systems, the beam waist w_0 and Rayleigh range z_R:

$$z_R = \frac{\pi w_0^2}{\lambda}, \quad w(z) = w_0\sqrt{1 + (z/z_R)^2} \tag{34}$$

For a 30 cm lens at 153 GHz ($\lambda = 2$ mm, $w_0 \approx 12$ cm):

$$z_R = \frac{\pi \times 0.12^2}{0.002} = 22.6 \text{ m} \tag{35}$$

$$\theta_{\text{div}} = \frac{\lambda}{\pi w_0} = 5.3 \text{ mrad} = 0.30^\circ \tag{36}$$

The beam remains collimated ($< \sqrt{2} \cdot w_0$ diameter) for $\sim$23 m, maintaining high power density throughout the near-field region.